Gondwana Research 86 (2020) 182–202

Contents lists available at ScienceDirect

Gondwana Research

journal homepage: www.elsevier.com/locate/gr

The Moroccan Anti-Atlas ophiolites: Timing and melting processes in an intra-oceanic arc-back-arc environment

F. Hodel [a,*], A. Triantafyllou [b,c], J. Berger [a], M. Macouin [a], J.-M. Baele [d], N. Mattielli [e], C. Monnier [f], R.I.F. Trindade [g], M.N. Ducea [c,h], A. Chatir [i], N. Ennih [i], J. Langlade [j], M. Poujol [k]

[a] Géosciences Environnement Toulouse (GET), Observatoire de Midi-Pyrénées, CNRS, IRD, Université Toulouse III Paul Sabatier, 14, Avenue Edouard Belin, 31400 Toulouse, France
[b] Department of Geology, University of Liège, Sart Tilman, Liège, Belgium
[c] Department of Geosciences, University of Arizona, Tucson, AZ 85721, USA
[d] Geology and Applied Geology Unit – Mining Geology, Université de Mons, 20, Place du Parc, B-7000, Belgium
[e] Department of Earth and Environmental Sciences – G-Time Laboratory, Université Libre de Bruxelles, 50 Avenue Franklin Roosevelt, 1050 Brussels, Belgium
[f] Laboratoire de Planétologie et Géodynamique – Nantes (LPGN), UFR Sciences et Techniques, Université de Nantes, UMR-CNRS 6112, France
[g] Instituto de Astronomia, Geofísica e Ciências Atmosféricas, Universitad de São Paulo, 05508-900 São Paulo, Brazil
[h] Faculty of Geology and Geophysics, University of Bucharest, Bucharest, Romania
[i] EGGPG, Département de Géologie, Faculté des Sciences, Université Chouaïb Doukkali, 24000 El Jadida, Morocco
[j] Microsonde Ouest, Ifremer–Centre de Bretagne, Technopole Brest Iroise, BP70, F-29280 Plouzané, France
[k] Univ Rennes, CNRS, Géosciences Rennes, UMR 6118, 35000 Rennes, France

A R T I C L E I N F O

Article history:
Received 31 January 2020
Received in revised form 22 May 2020
Accepted 23 May 2020
Available online 02 July 2020

Handling Editor: A. Festa

Keywords:
Neoproterozoic
SSZ
Ophiolite
Back-arc
U-Pb dating
Serpentinite
West African Craton

A B S T R A C T

The Moroccan Anti-Atlas orogenic belt encloses several Precambrian inliers comprising two major Neoproterozoic ophiolitic complexes: the Sirwa and Bou Azzer ophiolites. These ophiolites expose crustal and mantle units, thrusting over fragments of a long-lived intra-oceanic arc system. We present a detailed geochronological and petro-geochemical study of three mafic/ultramafic units of these two ophiolites: the Khzama sequence (Sirwa ophiolite) and the Northern and Southern Aït Ahmane sequences (Bou Azzer ophiolite). The crystallization of layered metagabbros from the Bou Azzer ophiolite (North Aït Ahmane sequence) has been dated here at 759 ± 2 Ma (U-Pb on zircons). This new age for the Bou Azzer ophiolite is similar to the formation of the Sirwa ophiolite (762 Ma) and suggests that both units formed during the same spreading event. Metabasalts of the three units show tholeiitic signature but with variable subduction-related imprints marked by LILE enrichments, HFSE depletions and variable Ti contents, similar to modern back-arc basin basalts (BABB). Their back-arc origin is also supported by the geochemical signature of ultramafic units showing very low contents in major and trace incompatible elements (Al_2O_3: 0.12–1.53 wt%, Ti: 3.5–64.2 ppm and Nb: 0.004–0.10 ppm), attesting of a highly refractory protolith. This is in agreement with the high Cr# (0.44–0.81) and low to intermediate Mg# (0.25–0.73) of their constitutive Cr-spinels. Dynamic melting models suggest that these serpentinites experienced intense and polyphased hydrous melting events, strongly influenced by supra-subduction zone SSZ-fluid influx and subduction-related melt percolation. Being particularly affected by these SSZ-melt/rock interactions and closer to arc units to the south, the Sirwa ophiolite and the South Aït Ahmane unit of the Bou Azzer ophiolite likely represent an early stage of the arc-back-arc system, which has been more influenced by the magmatic products of the arc activity compared to the North Aït Ahmane unit of the Bou Azzer ophiolite.

1. Introduction

Due to lithosphere recycling induced by plate tectonics, no oceanic lithosphere older than 220 Ma remains in place nowadays (Müller et al., 2008). Ophiolites are therefore the only available objects to investigate older oceanic lithosphere. A recent census by Furnes et al. (2015) highlights a great abundance of Neoproterozoic and early Cambrian ophiolites worldwide, mostly dated from 850 Ma to 500 Ma, testifying of a peculiar geodynamic activity at that time, marked by the demise of the Rodinia supercontinent and the further assembly of Gondwana. Most of these ophiolites are interpreted as remnants of supra-subduction lithosphere (e.g. Dilek and Furnes, 2011; Stern et al., 2012). They expose in places complete vertical sections of supra-subduction lithosphere, poorly accessible on modern active systems. Back- or fore-arc basins remnants can provide key information about the tectonic regime of the overriding plate (Heuret and Lallemand, 2005) and therefore, new insights into subduction dynamics. Therefore,

* Corresponding author.
E-mail address: florent.hodel@get.omp.eu (F. Hodel).

https://doi.org/10.1016/j.gr.2020.05.014
1342-937X/

these Neoproterozoic ophiolites offer unique opportunities to study crustal production, subduction zones dynamics (Triantafyllou et al., 2016, 2018; Walsh et al., 2012) and oceanic hydrothermal activity (Hodel et al., 2017, 2018), associated to this critical period of the Earth's history (e.g. Stern, 2005).

Recent ocean drilling campaigns emphasized the geochemical heterogeneity of supra-subduction systems and the diversity of igneous processes depending on arc vicinity, slab dynamics, mantle enrichment and melting process (Hochstaedter et al., 2001; Tollstrup et al., 2010; Reagan et al., 2017). These new views on modern subduction systems reveal that deciphering a geodynamic context with geochemical discrimination tools applied to metabasaltic ophiolitic rocks can be difficult (see MacLeod et al., 2013 for the debate on the Oman ophiolite). Hence, by exposing both mafic and ultramafic lithologies of a given lithosphere section, ophiolites are prime targets to understand subduction systems and explain their geochemical diversity.

The Moroccan Anti-Atlas hosts several Neoproterozoic inliers (erosional windows) comprising ophiolitic sequences that offer a unique opportunity to study these particular subduction settings (Bousquet et al., 2008). In the present study, we focus on the two main ophiolitic sequences exposed in the Anti-Atlas: the Sirwa ophiolite (e.g., Chabane, 1991; El Boukhari et al., 1992; Admou and Juteau, 1998), dated at 762 ± 2 Ma by Samson et al. (2004), and the Bou Azzer ophiolite (e.g. Leblanc, 1975; Bodinier et al., 1984; Naidoo et al., 1991; Ahmed et al., 2005, 2009). The age of the Bou Azzer ophiolite is still debated (El Hadi et al., 2010), the most commonly quoted age being a Rb/Sr age of 788 ± 10 Ma (Clauer, 1976), obtained on hornfels pelites collected close to meter-thick mafic sills.

Only a few studies treat of the ultramafic lithologies of these ophiolitic sequences (Leblanc, 1975; Ahmed et al., 2005; Gahlan et al., 2006; Hodel et al., 2017, 2018) and their petrology along with their geochemistry remain poorly constrained. Here we present a detailed petrological study of the ultramafic and the mafic units coupled with a geochronological study of the constitutive mafic rocks of the Sirwa and Bou Azzer ophiolites in order to better constrain their age and origin.

2. Geological context

The Moroccan ophiolites are part of the Precambrian basement cropping out in the central Anti-Atlas mountain range (Gasquet et al., 2005). These Precambrian inliers are exposed between two major fault zones (the South Atlas Fault, SAF and the Anti-Atlas Major Fault, AAMF), testify to the intense tectonic history that affected the northern margin of the West African Craton (WAC; Fig. 1a) during the Pan-African orogeny. Ophiolitic assemblages are exposed in two inliers: the Sirwa window to the west (Fig. 1b) and the Bou Azzer-El Graara inlier to the East (Fig. 1b).

Both inliers consist of several stacked tectonic blocks interpreted as dismembered parts of a Cryogenian (middle Neoproterozoic) oceanic supra-subduction system (e.g. Leblanc, 1975; Saquaque et al., 1989; Bodinier et al., 1984; Bousquet et al., 2008; Walsh et al., 2012; El Hadi et al., 2010; Soulaimani et al., 2018). These units were molded along the AAMF (Fig. 1b), surrounded and locally unconformably overlain by the Ediacaran (late Neoproterozoic) volcano-clastic deposits of the Ouarzazate Supergroup and late Ediacaran to Early Cambrian clastic sediments (Leblanc, 1981). Both inliers show strong field and petrological similarities that can be summarized as follows:

(1) *Neoproterozoic intra-oceanic arc remnants.* They consist of metavolcanic and -plutonic units, heterogeneous in composition (mafic to felsic), which are affected by a polyphased intrusive and deformation history.

In the Sirwa inlier, the Iriri-Tachakoucht-Tourtit arc complex is composed of andesitic to dacitic gneisses (Tachakoucht formation, Fig. 2a), intruded by hornblenditic magmas and hornblende gabbro dikes (mafic intrusions of Iriri, Fig. 2a). The contact between these intrusive bodies and the gneisses consists of leucocratic horizons, produced by the partial melting of the host gneiss. The orthogneiss of the Tachakoucht formation yields protolithic ages comprised between 735 ± 7 Ma and 725 ± 7 Ma (Thomas et al., 2002; Triantafyllou et al., 2016). The leucocratic horizons produced by their localized partial melting induced by the Iriri intrusions are younger, between 651 ± 5 Ma and 641 ± 5 Ma (see zircons' metamorphic overgrowths in, Thomas et al., 2002; Triantafyllou et al., 2016). The Iriri-Tachakoucht-Tourtit complex appears to be the product of several successive magmatic episodes with an intra-oceanic arc geochemical signature (Thomas et al., 2002; Triantafyllou et al., 2016, 2020).

In the Bou Azzer inlier, these arc remnants form a discontinuous strip along the southern border of the inlier and are mainly exposed within the Bougmane (Fig. 2b, south of the ophiolitic sequences) and Tazigzaout complexes (outside the area covered by the map in Fig. 2b). These highly metamorphosed complexes are composed of mafic gneisses (amphibolite) as well as granitic orthogneiss and granodioritic augen gneisses (see Triantafyllou et al., 2018). Triantafyllou et al. (2018, 2020) show that the Bougmane complex consists of 760–740 Ma heterogeneously mingled felsic-mafic orthogneiss intruded by several bodies of 710–690 Ma hornblendites, hornblende gabbros and garnet leucosomes. Garnet reaction zones form at the contact between different hornblende gabbro intrusions as a consequence of dehydration and dehydration melting under high pressure (garnet-present) granulite grade conditions (~800 °C, 10 kbar; Triantafyllou et al., 2018). These reactions induced by contact metamorphism are responsible for the formation of garnet-bearing leucosomes during incipient partial melting of hornblende-rich rocks. As well as for the Iriri-Tachakoucht-Tourtit arc complex of the Sirwa inlier, the geochemical and isotopic studies of D'Lemos et al. (2006) on the Tazigzaout complex and of Triantafyllou et al. (2018, 2020) on the Bougmane complex have shown that all these rocks are the product of a polyphased magmatic activity from a magmatic arc system located in an intra-oceanic domain.

(2) *Dismembered ophiolitic sequences* (main topic of this study). They are both stacked via early south dipping faults on the southern arc complexes previously described, the Iriri-Tachakoucht-Tourtit complex for the Sirwa sequence and the Bougmane complex for the Bou Azzer sequences.

The Sirwa ophiolitic sequence displays metagabbroic rocks, associated with several metabasaltic clusters interpreted as the remnants of a sheeted dyke complex (El Boukhari et al., 1992; Admou and Juteau, 1998). Ultramafic units are poorly exposed. They consist of small lenses of strongly deformed serpentinized spinel-harzburgites and dunites, locally associated with pyroxenites (Chabane, 1991; El Boukhari et al., 1992). This ophiolitic sequence is extensively tectonized, marked by tectonic contacts between most of its ophiolitic terms (see Fig. 2 in Triantafyllou et al., 2020). Three major tectonic slices were recognized in the studied area, whose sole appears systematically represented by soft serpentinite bands. These sliced and stacked units were subsequently dismembered and verticalized via sinistral transpressive deformation occurring during syn- to late-orogenic shearing along the Anti-Atlas Major Fault (Triantafyllou et al., 2012; Triantafyllou et al., 2020).

Geochemical studies carried out on the metabasaltic rocks of the Sirwa ophiolite show an SSZ (supra-subduction zone) affinity (e.g., El Boukhari et al., 1992) The intra-oceanic nature of this SSZ is supported by their highly positive εNd signatures (+7.5 to +8.8; Triantafyllou et al., 2020) which reflect an old depleted mantle source (but recently refertilized by subduction fluids and melts) without assimilation of WAC-derived continental material. The formation of this oceanic lithosphere was dated at 762 ± 2 Ma on ophiolitic plagiogranite dikes (U-Pb on zircon, Samson et al., 2004).

The Bou Azzer ophiolite was described in detail for the first time by Leblanc (1975). Here, we focus on the North and South Aït Ahmane

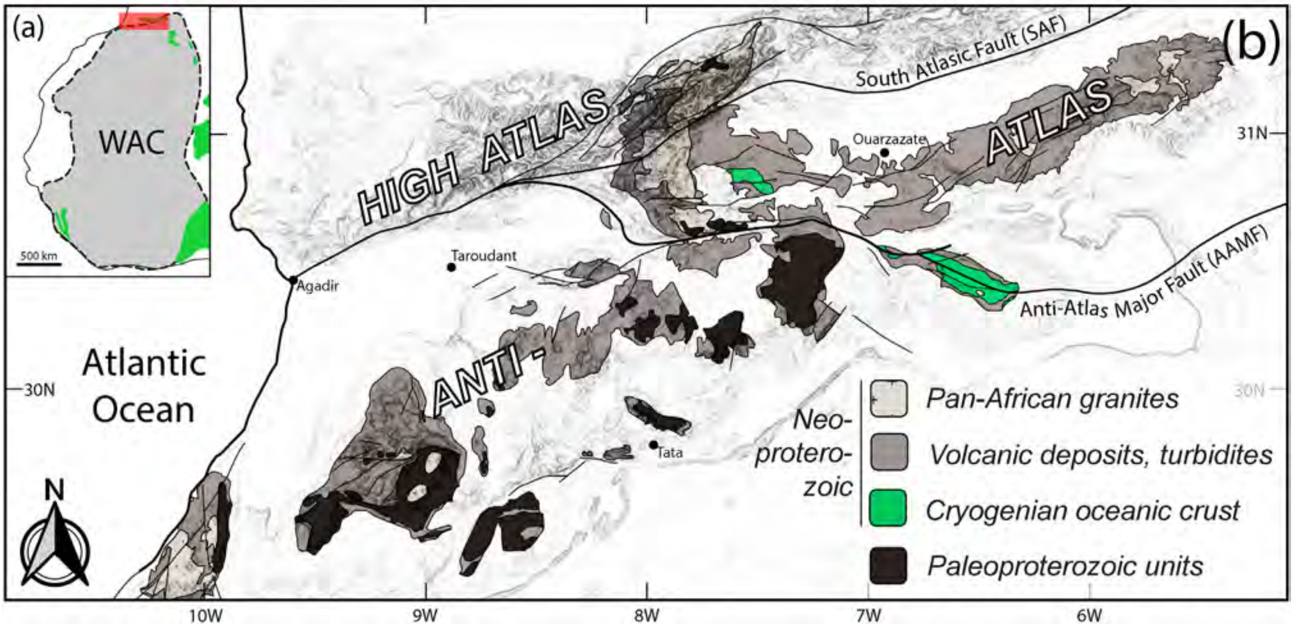

Fig. 1. Simplified geological maps. (a) Location of the studied area in relation to the West African Craton (WAC). Green parts represent the Pan-African orogenic belt. (b) Schematic map of the Precambrian inliers exposed in the Moroccan Anti-Atlas mountain belt (modified after Gasquet et al., 2008; basemap is Aster GDem 2.0 topographic data) showing the Sirwa and the Bou Azzer - El Graara inliers to the W and the E, respectively. (For interpretation of the references to colour in this figure legend, the reader is referred to the web version of this article.)

sequences, close to the eponym locality. It consists of a strongly tectonized and dismembered ophiolitic assemblage exposed in the inner part of Bou Azzer inlier (Fig. 2b). The architecture of the Bou Azzer ophiolite has been studied in detail by El Hadi et al. (2010). These authors showed that the ophiolite has been structured as a complex anticlinal-shaped structure resulting from its evolution through subduction to collisional tectonics (see also Bousquet et al., 2008 and Admou et al., 2013, for more precise descriptions of the Bou Azzer ophiolite structure). The mantle section is the most represented (~70% of the sequence, Fig. 2b) with serpentinites deriving from spinel-harzburgites and rare dunitic lenses. These largely dominant residual lithologies are associated with rare occurrences of pyroxenites and chromite pods. Mafic units are mainly metagabbros (layered and isotropic). Isotropic metagabbros are strongly deformed and retrogressed to amphibolite. Layered gabbros are marked by planar variations in modal proportions that are transposed in the main foliation trend (Fig. 3a, b). Metabasalts are exposed as metric dykes and/or undistinguished massive units. Ductile deformation is also marked in the form of boudinaged dykes along with a slight foliation subparallel to boudins. These metabasaltic massifs are interpreted as the relics of the sheeted dykes' complex and as pillow lavas occasionally capping ophiolitic sequence (Leblanc, 1975, 1981). The basaltic lavas present a SSZ affinity (Bodinier et al., 1984; Naidoo et al., 1991) and as for the Sirwa ophiolitic basalts, their Nd isotopic signature shows positive values (εNd ranging from +6.3 and +8.1; Triantafyllou et al., 2020) in agreement with a juvenile mantle source. The Bou Azzer ophiolite was described either as a fragment of a back-arc lithosphere (Bodinier et al., 1984; Triantafyllou et al., 2018) or as a fore-arc (Naidoo et al., 1991). The only petro-geochemical study conducted on the Bou Azzer serpentinites concerns the discovery of a fossil black smoker type hydrothermal system in the North Aït Ahmane unit (Hodel et al., 2017, 2018). Other studies carried out on these ultramafic rocks investigated spinels chemistry in serpentinites (Ahmed et al., 2005, 2009; Gahlan et al., 2006; Hodel et al., 2017). These studies tend to confirm the SSZ affinity of these oceanic remnants. The age of this section of oceanic lithosphere is still debated. No robust igneous age is available yet. El Hadi et al. (2010) proposed an age of 697 ± 6 Ma (U-Pb on zircons) for a gabbroic rock belonging to the Bougmane complex that they interpreted as belonging to the ophiolitic sequence based on their tectonic model. However, these rocks were recently re-interpreted as the root of the Bougmane arc complex based on their geochemical signature, the nature of its constitutive lithologies and, its high grade metamorphic evolution (up to granulite facies; Triantafyllou et al., 2018, 2020). The 697 ± 8 Ma age obtained by El Hadi et al. (2010) is equivalent, within errors, to the 710–690 Ma ages obtained for hornblendites and related rocks of the Bougmane complex (D'Lemos et al., 2006; Triantafyllou et al., 2018). We consider that the sample dated by El Hadi et al. (2010) does not constrain the timing of oceanic spreading as represented by the Bou Azzer ophiolite at Aït Ahmane but rather characterize the second igneous phase of the Bougmane oceanic arc (Triantafyllou et al., 2018).

(3) *Late Cryogenian dioritic, granodioritic to granitic intrusions* cutting across the ophiolitic units were described in both Sirwa and Bou Azzer inliers. Their emplacement ages were constrained with U-Pb geochronology on magmatic zircon grains and range between 660 and 640 Ma (Inglis et al., 2004; El Hadi et al., 2010; Walsh et al., 2012; Blein et al., 2014; Triantafyllou et al., 2016).

3. Field relations and samples description

Representative samples of metabasalts, metagabbros (mafic units) as well as serpentinized peridotites (ultramafic units) were collected from both the Sirwa and Bou Azzer ophiolites (see Fig. 2a, b).

For the Sirwa ophiolite, sixteen serpentinites, four metagabbros and nine metabasalts samples were collected in the Khzama area. The Khzama serpentinites were sampled in two ultramafic massifs located northward of the Amassine village (SRW series) as well as two other massifs exposed on both sides of the Tourtit village (KK series). Most of the metabasaltic and metagabbroic rocks were sampled in the western Amassine valley. Additional mafic samples were collected from both central and eastern valleys of the area to ensure representativity and coverage on the Sirwa ophiolitic sequence (Fig. 2a).

Two main mafic-ultramafic assemblages were recognized and sampled in the Bou Azzer ophiolite (Fig. 2b): (i) the Northern Aït Ahmane unit is located in the central part of the Bou Azzer-El Graara inlier. It is

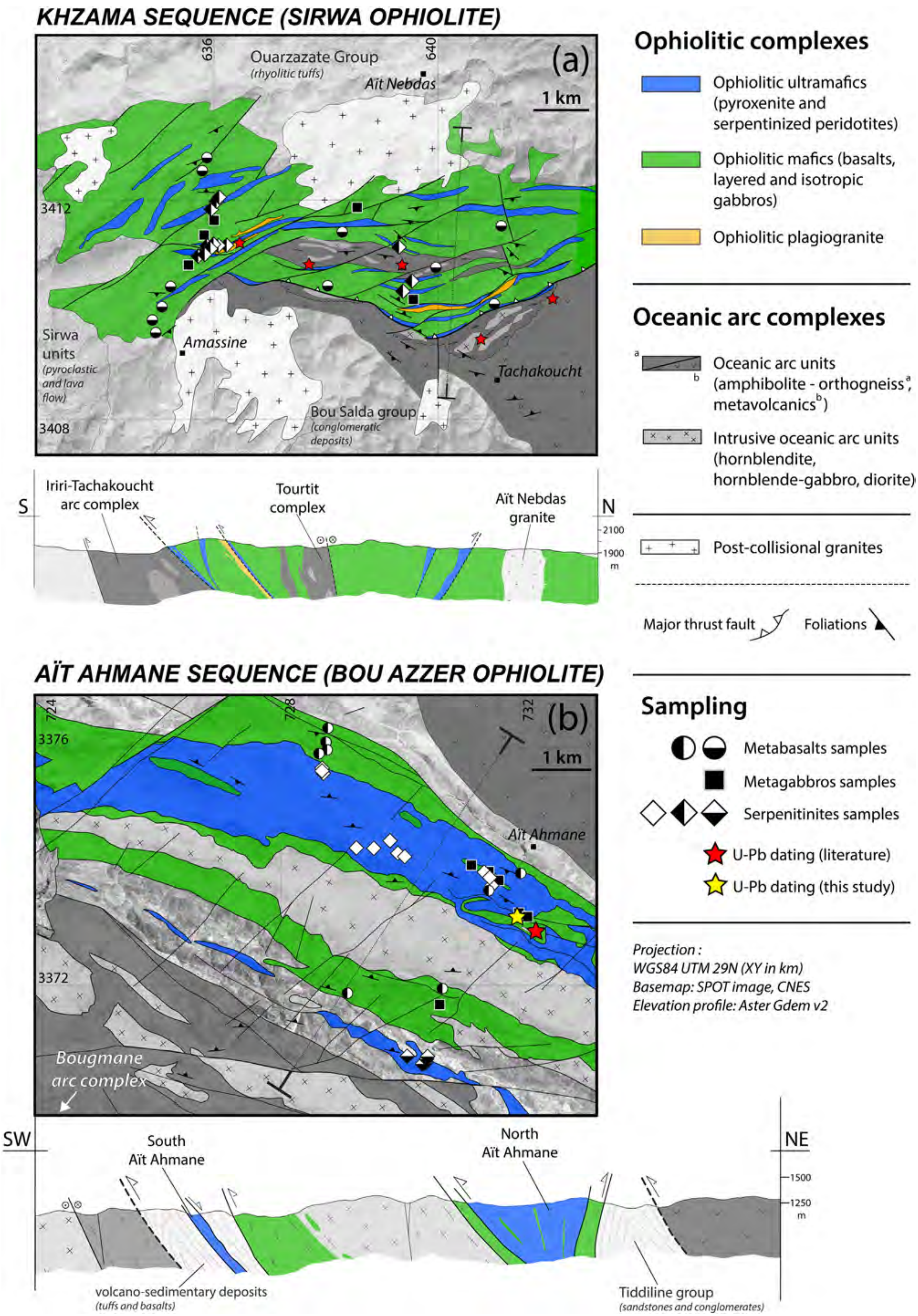

KHZAMA SEQUENCE (SIRWA OPHIOLITE)
(a)
636
640
1 km
Ouarzazate Group
(rhyolitic tuffs)
Aït Nebdas
3412
3408
Sirwa units
(pyroclastic and lava flow)
Amassine
Tachakoucht
Bou Salda group
(conglomeratic deposits)
S
N
Iriri-Tachakoucht arc complex
Tourtit complex
Aït Nebdas granite
2100
1900
m
Ophiolitic complexes
Ophiolitic ultramafics (pyroxenite and serpentinized peridotites)
Ophiolitic mafics (basalts, layered and isotropic gabbros)
Ophiolitic plagiogranite
Oceanic arc complexes
Oceanic arc units (amphibolite - orthogneiss^a, metavolcanics^b)
Intrusive oceanic arc units (hornblendite, hornblende-gabbro, diorite)
Post-collisional granites
Major thrust fault
Foliations
AÏT AHMANE SEQUENCE (BOU AZZER OPHIOLITE)
(b)
724
728
732
3376
3372
1 km
Aït Ahmane
Bougmane arc complex
Sampling
Metabasalts samples
Metagabbros samples
Serpenitinites samples
U-Pb dating (literature)
U-Pb dating (this study)
Projection :
WGS84 UTM 29N (XY in km)
Basemap: SPOT image, CNES
Elevation profile: Aster Gdem v2
SW
NE
South Aït Ahmane
North Aït Ahmane
1500
1250
m
volcano-sedimentary deposits
(tuffs and basalts)
Tiddiline group
(sandstones and conglomerates)

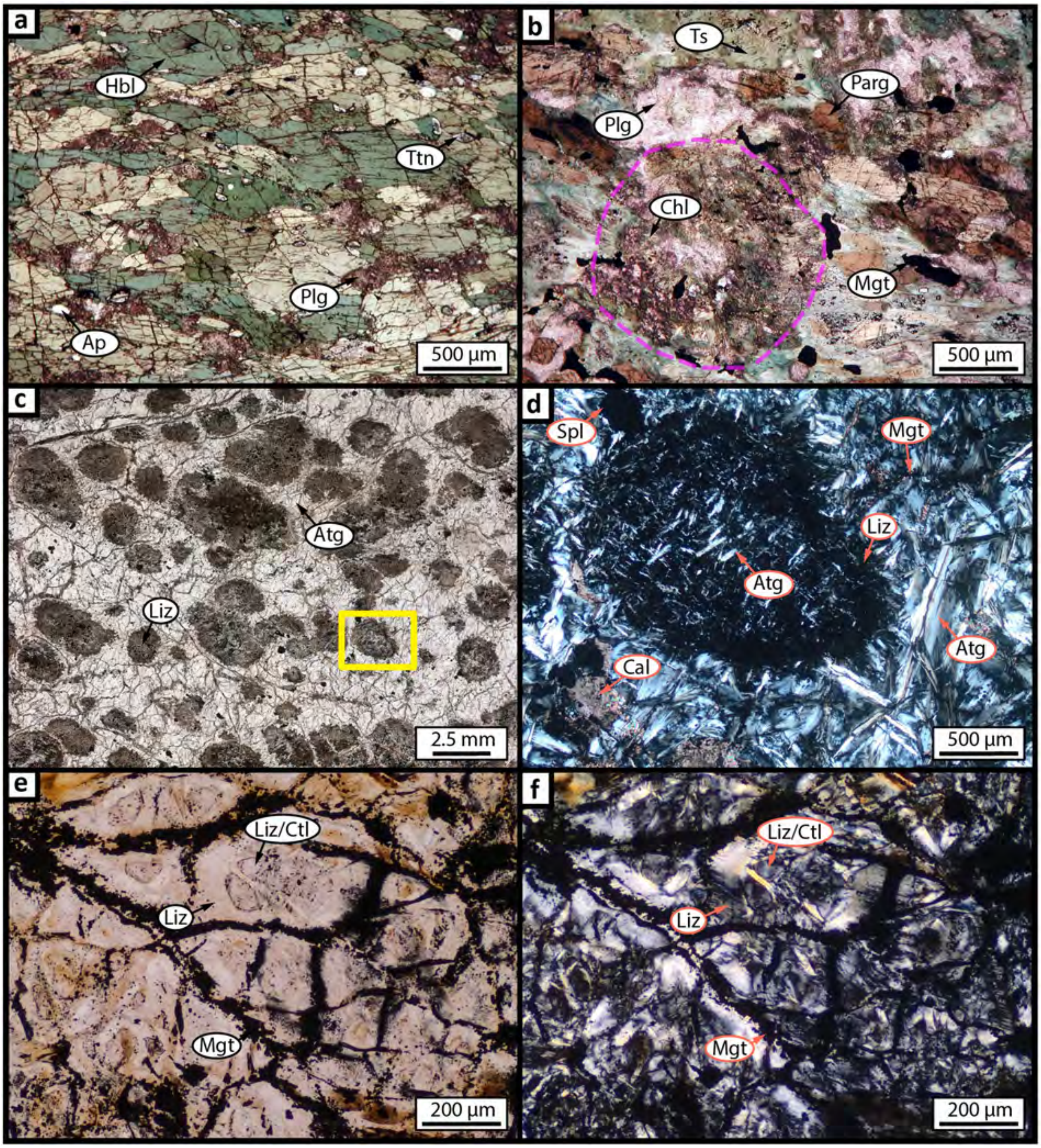

Fig. 3. (a) Microphotograph of melanocratic layer in L72 layered metagabbro used for U-Pb dating (hornblende + retrogressed plagioclase + accessory apatite and titanite). (b) Microphotograph of L68 isotropic metagabbro showing relics of high grade paragenesis (i.e. pargasite and see dashed pink line for garnet pseudomorphosis). (c) High resolution scan of a thin section portion of a South Aït Ahmane serpentinite showing the dark lizardite/chrysotile nodules in clearer antigorite (in plane-polarized light). The yellow rectangle corresponds to the zoomed view on the photomicrograph to the right (in d). (d) Photomicrograph of a dark lizardite nodule in clearer interpenetrated antigorite blades. Note the presence of calcite in the left down corner. (e, f) Photomicrographs of a North Aït Ahmane serpentinite displaying a pseudomorphic lizardite/chrysotile mesh texture with abundant magnetite concentrated in mesh rims (e in plane-polarized light and f in cross-polarized light). Abbreviations correspond to: Hbl: hornblende, Plg: plagioclase, Ttn: titanite, Ap: apatite, Chl: chlorite, Liz: lizardite, Atg: antigorite, Ctl: chrysotile, Spl: spinel, Mgt: magnetite, Cal: calcite. (For interpretation of the references to colour in this figure legend, the reader is referred to the web version of this article.)

bordered by isotropic metagabbroic and metabasaltic units to the North and by isotropic and layered metagabbros as well as metabasalts and the intrusive Aït Ahmane quartz-diorite to the South (Fig. 2b); (ii) The Southern Aït Ahmane unit consists of an alignment of small dismembered serpentinite lenses outcropping to the south of the inlier into Upper Cryogenian volcano-sedimentary formations (Admou et al.,

Fig. 2. (a) Simplified geological map and cross section of the Sirwa ophiolite (Khzama sequence) modified from Triantafyllou et al. (2016). (b) Simplified geological map and cross section of the Aït Ahmane sequences of the Bou Azzer ophiolite and associated plutono-metamorphic (intra-oceanic arc) units to the south (combining field information of this study and from Admou et al., 2013). Background gray scale images for are grayscale SPOT images product (CNES) and elevation profiles were extracted from Aster Gdem v2 topographical data. KMZ versions of these maps including samples locations have been generated using Geolokit app (Triantafyllou et al., 2017) and can be found in the Supplementary Materials 1.

2013). We discarded serpentinites displaying obvious alteration features in the field and conducted our sampling campaign away from zones were carbonation and/or hydrothermal overprint have been described by Hodel et al. (2017, 2018) for the North Aït Ahmane unit. Nine metabasalts and seven metagabbros were sampled in the Northern Aït Ahmane area. The North Aït Ahmane ultramafic unit was already sampled by Hodel et al. (2018) who studied variously hydrothermalized serpentinites and associated massive magnetite veins. We sampled five additional serpentinites from this unit. Sixteen serpentinites, two metabasalts and one metagabbro were also sampled in the Southern Aït Ahmane unit following a N-S profile (Fig. 2b). All the analytical methods and protocols are detailed in the appendices (see A.1. for Analytical methods).

4. Petrography and mineral chemistry

4.1. Mafic units

Metagabbroic units from the Khzama (Sirwa) and Aït Ahmane (Bou Azzer) ophiolitic units consist of amphibolites with fine- to medium-grained equigranular, granoblastic texture. Isotropic as well as layered metagabbros were observed in both units. The latter are characterized by centimetric to pluri-centimetric layering with variable plagioclase-amphibole modal proportions (Fig. 3a).

The Khzama metagabbros are made of tschermakitic amphibole (Mg# > 0.53, Si <6.5 apfu, see table X) and retrogressed andesine-oligoclase plagioclase (xAb ~ 60–80 mol%; xAb = Na/[Na + Ca + K] on molar basis) with accessory titanite-ilmenite, clinozoisite, apatite and occasional carbonate and quartz. The Aït Ahmane metagabbros share numerous petrographical similarities with the Khzama samples (Fig. 3a, b). They contain calcic amphibole with tschermakitic to Mg-hornblende composition (Mg# > 0.51, xSi_A ranging between 6.2 and 7.5 *apfu*; Leake et al., 2004) with few brownish cores with pargasitic composition (see Supplementary Material 2 for EPMA analyses). Retrogressed plagioclases range from andesine to albite compositions (48 < xAb < 91 mol%). Accessory phases are titanite, apatite, zircon and magnetite. Few metagabbros show relics of higher-grade pressure-temperature conditions marked by garnet pseudomorphosis (now totally retrogressed in chlorite-amphibole assemblage; Fig. 3b) along with amphibole cores with pargasitic compositions.

4.2. Ultramafic units

Serpentinites from the Khzama unit display a non-pseudomorphic texture, composed of interpenetrating antigorite blades (serpentinites varieties were determined using RAMAN spectroscopy, see Appendix A.1.1) (Fig. 3c, d). Some bastites (serpentinized pyroxenes) are sometimes recognizable through preserved original cleavages, often highlighted by alignments of magnetite grains. A darker phase occurring between antigorite blades is composed of a lizardite/chrysotile assemblage (Fig. 3c, d). In few samples, this lizardite/chrysotile assemblage forms circular nodules that reach several hundreds of micrometers in diameter (Fig. 3c, d). Given the degree and texture of serpentinization, it is almost impossible to determine the modal composition of the former peridotite.

Serpentinites from the South Aït Ahmane unit display similar petrographic characteristics to those from the Khzama unit. They are also mainly composed of interpenetrated antigorite blades (Fig. 3c, d) but lizardite/chrysotile darker nodules are much more present, even at the macroscopic scale (measuring from 0.5 to 4 mm, Fig. 3c, d). When compared to the serpentinites from the two other units, they are richer in carbonate phases (Fig. 3d). Carbonates are frequently associated with chrysotile in late veins or form patches into the antigoritic matrix (Fig. 3d).

Finally, serpentinites from the North Aït Ahmane unit display a pseudomorphic texture with a serpentine mesh formed after olivine retrogression (Fig. 3e, f) and bastites formed after orthopyroxene (about 10 to 20% of the modal composition).

Spinel is the only pristine mineral preserved from serpentinization in all the studied ultramafic rocks. Spinel grains are very weakly altered in the Khzama and South Aït Ahmane serpentinites despite the fact that antigorite is the largely dominant serpentine variety reported in these

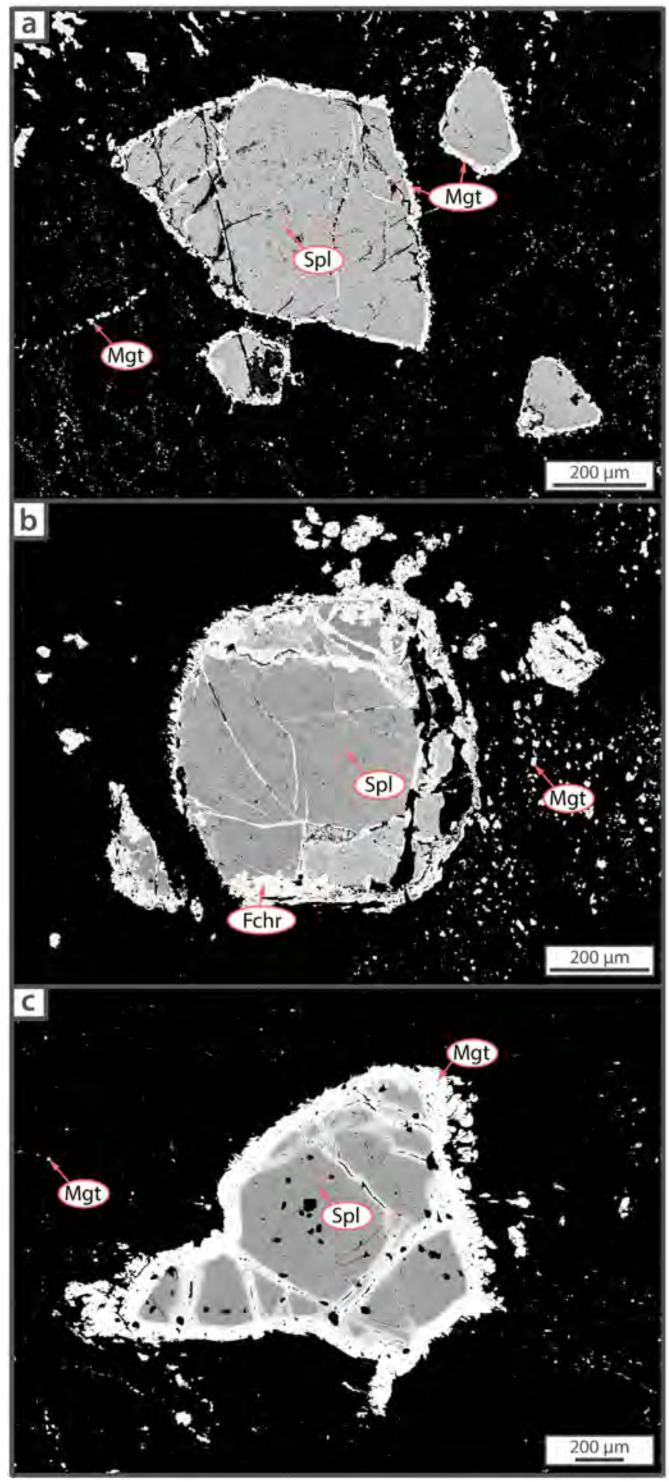

Fig. 4. BSE (Back Scattered Electron) images of euhedral to subhedral spinel grains partially altered to ferritchromite and Cr(Ni)-rich magnetite (a) from the Khzama serpentinites (b) from the South Aït Ahmane serpentinites and (c) from the North Aït Ahmane serpentinites.

serpentinites. Spinel grains are euhedral to subhedral. They are rimmed by a thin ferritchromite and/or Cr (+Ni)-bearing magnetite aureole (Fig. 4a, b). The degree of alteration is much more variable in the North Aït Ahmane serpentinites, mainly due to the intense hydrothermal activity that affected these serpentinites (Hodel et al., 2017, 2018). For mineral chemistry, we only considered the less affected samples and analyzed only the preserved spinel cores of the least altered grains (Fig. 4c).

Unaltered spinel cores show intermediate to high Cr# (Cr# = Cr/[Cr + Al] = 0.44–0.81) and low to high Mg# values (Mg# = [Mg/(Mg + Fe^{2+})] = 0.25–0.73) (Fig. 5a, see also Supplementary material 3). Spinels from the Khzama serpentinites display a narrow Cr# and Mg# range, varying from 0.68 to 0.81 and 0.26 to 0.57, respectively. Spinels from the South and North Aït Ahmane units present more variable compositions with Cr# and Mg# ranging from 0.44 to 0.79 and 0.34 to 0.73, respectively. For the three units, these compositions point to a highly depleted protolith (more than 25% of melt extraction in most cases; Arai, 1994) hence, corresponding to the composition of spinel found in subduction related peridotites (Fig. 5a). Spinels from Aït Ahmane serpentinites have very low TiO_2 contents (<0.1 wt%) consistent with a highly depleted precursor while the spinels from the Khzama serpentinites are characterized by higher TiO_2 contents (0.10–0.26 wt%), reflecting prior-serpentinization melt/rock interactions, i.e. refertilization processes (Fig. 5b).

5. Whole-rock chemistry

5.1. Metabasalts

Major and trace elements concentrations measured on mafic rocks are provided in Supplementary material 4.

5.1.1. Major elements

Metabasaltic samples from the Khzama and Aït Ahmane ophiolitic units are subalkaline basalts and basaltic andesites (SiO_2 content 47–54 wt%; median value at 50.3 wt%; $Na_2O + K_2O$ < 5.9 wt%; median at 4.6 wt%). They show tholeiitic affinity with only a few samples displaying a calk-alkaline signature (FeO*/MgO ranges between 0.9 and 2.6 wt%; median at 2.1 wt%). Subalkaline signature is also confirmed by their low Nb/Y ratios (<0.26; Winchester and Floyd, 1977) except for one sample (AH25). The Aït Ahmane metabasalts show relatively low TiO_2 contents which typically correspond to an arc-related Ti-poor lavas signature. The Sirwa metabasalts show higher Ti values pointing to a transitional composition between MORB and back-arc mafic lavas.

5.1.2. Trace element

Two types of metabasalts were distinguished based on their REE patterns. Both types occur in the Sirwa and the Aït Ahmane ophiolitic massifs:

(i) The first type is characterized by relatively low REE contents (6 to 15 times the chondritic values; median at 8), flat MREE to HREE pattern ($[Dy/Yb]_N$ median at 0.99; Fig. 6a) and flat to depleted LREE profiles ($[La]_N$ values range from 6.4 to 9.1) comparable to N-MORB signature. They are enriched in LILE (Large Ion Lithophile Elements: Cs, Rb, Ba, Th) compared to NMORB reference value ($[Ba]_{N.NMORB}$ and $[Th]_{N.NMORB}$ ranging from 12.3 to 49.0 and 1.6 to 3.0, respectively with median values at 13.9 and 2.5) (Fig. 6b). Sr contents are variable but correlated with Eu variations and reflecting plagioclase fractionation. HFSE (High Field Strength Elements) concentrations are low compared to NMORB. Along with the REE signature described above, these rock analyses are consistent with a mantle source strongly depleted in incompatible elements and/or affected by high degrees of mantle melting. Their Th/Nb ratios are comprised between 0.03 and 0.42, similar to the expected N-MORB value (~0.04; Sun and McDonough, 1989).

(ii) The second type is marked by higher REE abundances (15 to 35 times the chondritic values; median at 22), patterns showing significant fractionation between MREE and HREE ($[Dy/Yb]_N$ median at 1.34) and generally higher LREE content ($[La]_N$ range from 19.3 to 82.4; Fig. 6c, d). These REE signatures are very comparable to island arc tholeiitic basalt patterns (Fig. 6c). The N-MORB-normalized multi-elements patterns (Fig. 6d) show

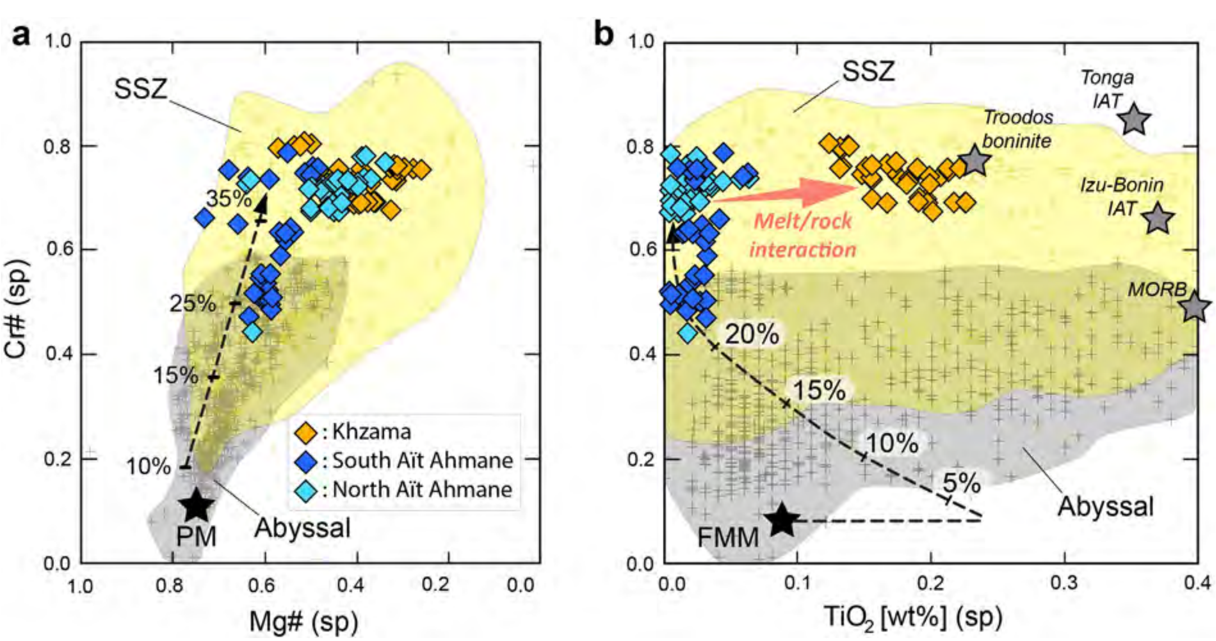

Fig. 5. Spinel compositions in serpentinites from the Aït Ahmane (Bou Azzer) and Khzama (Sirwa) complexes (104 grains of 23 samples). (a) Compositional relationship between Cr# (= Cr/[Cr + Al]) and Mg# (=Mg/[Mg + Fe^{2+}]) of spinels in the Aït Ahmane and Khzama serpentinites. Only primary cores analyses are represented here and have been considered for petrogenetic interpretations. (b) Compositional variations of Cr# vs TiO_2 (wt%) content in spinels (after Pearce et al., 2000). Abyssal peridotites field is from Warren (2016), SSZ (Supra Subduction Zone) peridotites field is from Ishii et al. (1992) and Parkinson and Pearce (1998). Partial melting trend is from Arai (1994).

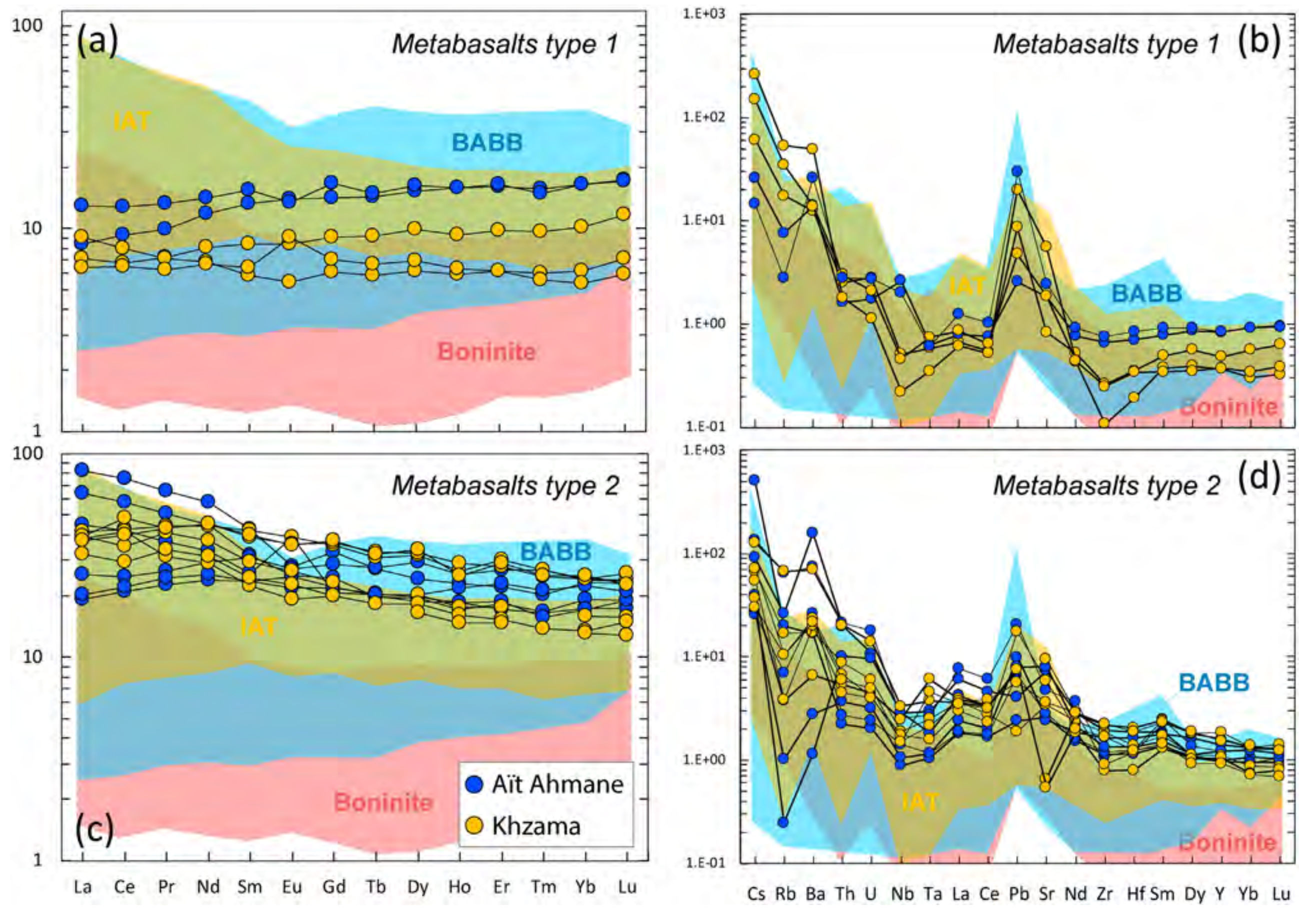

Fig. 6. (a, c) Chondrite-normalized REE patterns of the Khzama and the Aït Ahmane metabasalts. Chondrite values are from Barrat et al. (2012). (b, d) NMORB-normalized multi-element patterns for the Khzama and the Aït Ahmane metabasalts. NMORB values are from Sun and McDonough (1989). IAT (Island Arc Tholeiite) and BABB (Back-Arc Basin Basalts) compositions are from PetDB (https://www.earthchem.org/petdb) and boninites compositions are from the GEOROC database (http://georoc.mpch-mainz.gwdg.de).

higher values in incompatible elements than for type-1 metabasalts. Enrichments in LILE elements are variable but mostly above MORBs ($[Ba]_{N.NMORB}$ and $[Th]_{N.NMORB}$ ranging from 1.2 to 158.4 and 1.6 to 21.4, respectively with median values at 20.2 and 6.0). Most samples show negative anomalies in Nb-Ta ($[Nb]_{N.NMORB}$ values vary between 0.9 and 3.3) and slight negative anomalies in Zr-Hf ($[Zr]_{N.NMORB}$ values: 0.7–2.2). The Th/Yb ratio is a useful proxy to quantify the amount of slab-derived component into depleted MORB mantle (Pearce and Stern, 2006). Both types of metabasalts show a strong influence of subduction component to the MORB array (ranges of Th/Yb: 0.07–1.07 for Nb/Yb: 0.6–3.4; range of Ti/Yb: 1208–4227 and Zr/Yb: 11–56 for La/Yb: 0.7–4.9; see Fig. 7a, b, c).

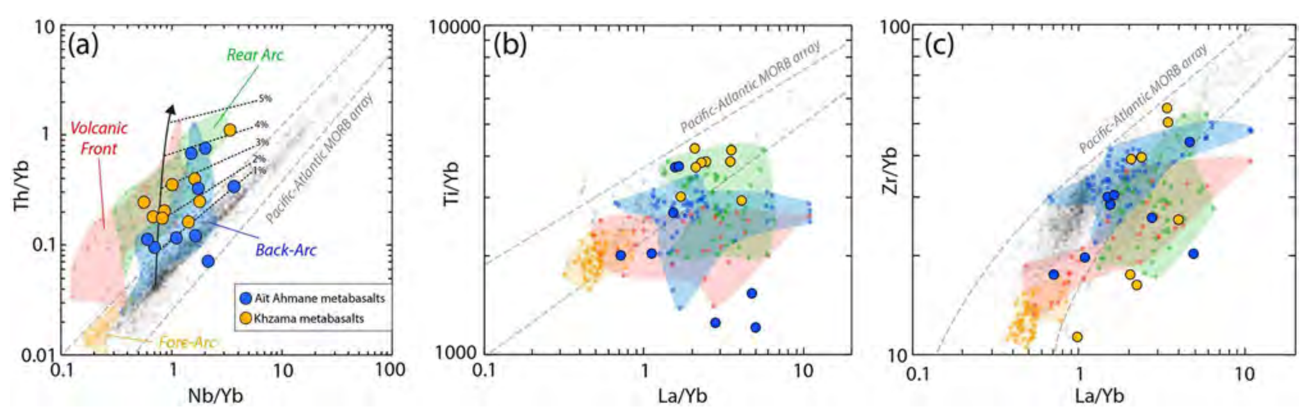

Fig. 7. Th/Yb, Ti/Yb and Zr/Yb versus Nb/Yb or La/Yb diagrams for the Aït Ahmane and Khzama metabasalts. Note the departure from the mantle array indicating the presence of a subduction component (higher Th/Yb, lower Ti/Yb and Zr/Yb; see text for details). Fields of Izu-Bonin-Mariana (IBM) volcanic front (red) and back-arc (blue), rear arc (green) and forearc (yellow) basalts composition are gathered from PetDB (https://www.earthchem.org/petdb). Percentages of subduction contamination are from Pearce (2008). The mantle array extends from below normal-mid ocean ridge basalt (N-MORB) through intraplate basalts to ocean island basalts (OIB). Light gray dots are MORB values gathered from PetDB (https://www.earthchem.org/petdb). (For interpretation of the references to colour in this figure legend, the reader is referred to the web version of this article.)

5.2. Metagabbros

5.2.1. Major elements

Metagabbros in Khzama and Aït Ahmane ophiolitic sequences show relatively low SiO_2 (41.8–51.1 wt%) contents, high MgO (median at 11.6 wt% and range between 7.04 and 24.6 wt%) and CaO (10.1–19.9 wt%) contents along with relatively low TiO_2 contents (0.72 wt% TiO_2, in average).

5.2.2. Trace element

Two types of metagabbros can be distinguished (Fig. 8): (i) Type 1 metagabbros have only been observed in the northern Aït Ahmane ophiolitic sequence. They show relatively high content in incompatible elements (REE concentrations are 16 to 27 chondritic values). REE patterns are relatively flat with a slight depletion in LREE ($[La/Sm]_N$ ranging between 0.41 and 0.69; $[Gd/Yb]_N$ between 1.06 and 1.18) (Fig. 8a). Their trace elements composition is very similar to N-MORB, with relative enrichment in Cs, Rb, Ba, Nb and Pb (Fig. 8b). They show typical gabbro signature from the middle to upper crustal section of oceanic crust (see comparison with Samail 'high-gabbros' on Fig. 8a). (ii) Type 2 metagabbros are marked by lower abundances in REE and other incompatible elements (REE between 0.1 and 1 time chondritic values; Nb: 0.01–2.95 ppm, Zr: 0.01–0.05 ppm, Y: 0.03–0.19 ppm) (Fig. 8). REE patterns show strong LREE depletion relative to MREE ($[La/Sm]_N$ ratios ranges between 0.18 and 0.83) and flat MREE-HREE trends ($[Gd/Yb]_N$ ratios between 0.85 and 1.17; Fig. 8a). Slight positive Eu anomalies ($[Eu/Eu^*]_N$: 1.03 to 1.72) are correlated with Sr contents and attributed to plagioclase accumulation. Type 2 metagabbros show typical cumulative signature, similar to those from the Samail lower to middle crust gabbros (Fig. 8a).

The layered metagabbro dated in this study (sample L72, see Section 6) belongs to the type 1 group. Both type 1 and type 2 metagabbros from the

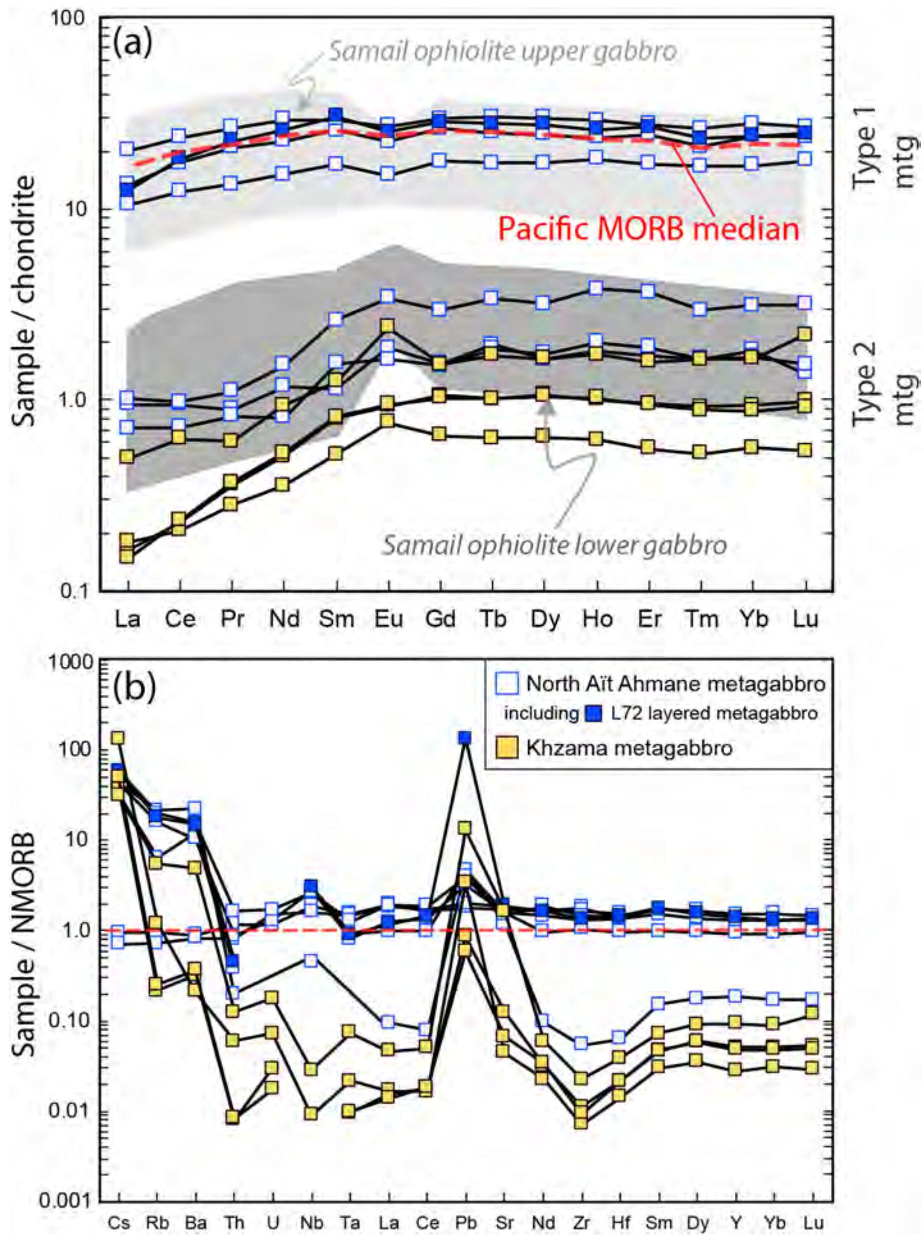

Fig. 8. (a) Chondrite-normalized REE patterns and (b) N-MORB-normalized multi-element patterns for the Khzama and of the northern Aït Ahmane metagabbroic rocks. Dated layered metagabbro (sample L72) is represented to show its NMORB affinity. Chondrite and NMORB normalizing values are from Barrat et al. (2012) and Sun and McDonough (1989) respectively. Samail ophiolites' (Oman) low and upper crust gabbro fields are from Pallister and Knight (1981) and Kelemen et al. (1997). Median composition of Pacific Oceanic Ridge Basalt (red dashed line) is calculated based on PetDB (https://www.earthchem.org/petdb) database. (For interpretation of the references to colour in this figure legend, the reader is referred to the web version of this article.)

Sirwa and the Bou Azzer ophiolite show oceanic-like signature, attesting of their genetic link with the ophiolitic sequence. Moreover, they display different geochemical signature compared to mafic rocks forming the oceanic arc complex to the south (e.g. Bougmane complex in Bou Azzer and Iriri complex in Sirwa; Triantafyllou et al., 2018). Specifically, type 1 and type 2 ophiolitic metagabbros are characterized by rather low La/Yb ratios (mean value at 0.42 and range between 0.17 and 0.70) compared to their arc-related counterpart (mean value at 1.68 and range from 1.05 to 3.1).

5.3. Serpentinites

Major and trace elements concentrations measured in ultramafic rocks are provided in Supplementary material 5.

5.3.1. Major elements

All the analyzed serpentinites show high LOI (Loss On Ignition) values, from 11.3 to 12.9 wt%, reflecting the high degree of serpentinization. Whole-rock major oxides contents were recalculated on a volatile-free basis in order to compare our results with the compositions reported for other serpentinites and variously serpentinized peridotites in the literature (Figs. 9 and 10).

Most of the analyzed serpentinites plots slightly under the mantle array (Jagoutz et al., 1979; Hart and Zindler, 1986) in a MgO/SiO_2 versus Al_2O_3/SiO_2 diagram (Fig. 9). Such feature is usual for highly serpentinized peridotites. It is explained either by Mg loss during low temperature seafloor alteration (Snow and Dick, 1995; Niu, 2004; Kodolányi et al., 2012; Deschamps et al., 2013) or by Si addition through fluid/rock interactions (e.g., Bach et al., 2004; Harvey et al., 2014; Boschi et al., 2013; Malvoisin, 2015). Nonetheless, this alteration signature is not dramatic in our samples, making reasonable to use MgO and SiO_2 concentrations as fertility indicators for their ultramafic protoliths. Most of the Khzama and Aït Ahmane serpentinites display a rather narrow range of high MgO/SiO_2 and low Al_2O_3/SiO_2 ratios varying from 0.96 to 1.08 and 0.03 to 0.016 respectively, characteristic of highly depleted peridotites. Three samples from the Khzama and the North Aït Ahmane units stand out by showing higher Al_2O_3/SiO_2 (0.034 for the sample from Khzama and 0.023 and 0.028 for the samples from Aït Ahmane) for similar MgO/SiO_2 (0.94 for the sample from Khzama and 0.98 for the samples from Aït Ahmane) testifying to a less depleted (or more refertilized) protolith for these three samples.

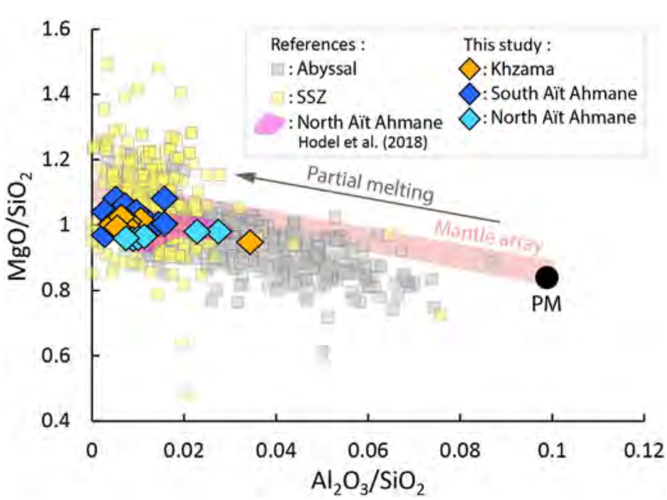

Fig. 9. MgO/SiO_2 vs. $Al2O_3/SiO_2$ ratios for the Khzama and Aït Ahmane (South and North) serpentinites. The pink domain corresponds to the North Aït Ahmane variously hydrothermalized serpentinites of the Hodel et al. (2018) study. Data for abyssal peridotites are from Snow and Dick (1995), Casey (1997), Niu (2004), Paulick et al. (2006), Godard et al. (2008), Augustin et al. (2012), Boschi et al. (2013), Andreani et al. (2014), Chen et al. (2015). Data for SSZ (Supra Subduction Zone) peridotites are from Ishii et al. (1992), Parkinson and Pearce (1998), Pearce et al. (2000), Savov et al. (2005, 2007), Marchesi et al. (2006, 2009) Kodolányi et al. (2012). Mantle array is from Jagoutz et al. (1979) and Hart and Zindler (1986). Primitive mantle values are from McDonough and Sun (1995). (For interpretation of the references to colour in this figure legend, the reader is referred to the web version of this article.)

Khzama and Aït Ahmane (North and South units) serpentinites are Al-poor (0.12–0.69 wt% for most of the samples and 1.02–1.53 wt% for the three samples that display higher Al_2O_3/SiO_2 ratios mentioned above, Fig. 10a). They show a wide range of MgO content (from 42.13 to 45.63, 41.61 to 45.73 and 41.84 to 43.73 wt% for the Khzama, South Aït Ahmane and North Aït Ahmane respectively), possibly reflecting either diverse protolith fertility or Mg loss during low temperature seafloor alteration (e.g., Snow and Dick, 1995; Niu, 2004). FeO_{Total} is highly variable (7.31–13.72 wt%, 6.32–10.22 wt% and 9.52–13.56 wt% for Khzama, South Aït Ahmane and North Aït Ahmane respectively). Hodel et al. (2017, 2018) showed that the hydrothermal activity affecting the North Aït Ahmane serpentinites led to an important iron mobilization in the serpentinites (see pink domain in Fig. 10b), involved in the precipitation of massive magnetite veins in cracks (see also Gahlan et al., 2006).

Whole-rock CaO content is known to be strongly affected by the serpentinization and associated carbonation reactions (Miyashiro et al., 1969; Coleman and Keith, 1971; Janecky and Seyfried, 1986; Palandri and Reed, 2004; Iyer et al., 2008). The carbonation of the South Aït Ahmane antigoritic serpentinites (Fig. 3d) results in high to very high CaO concentrations (0.04–7.64 wt%, Fig. 10c). The serpentinites from the Khzama and North Aït Ahmane units, which do not exhibit petrographic evidence of carbonation, show lower CaO concentrations, comprised between 0.03 and 0.96 wt%. These latter values are consistent with the harzburgitic and dunitic nature of their protolith. SiO_2 contents are also variable (42.31–45.00 wt%, 40.67–47.06 wt% and 43.50–44.77 wt% for Khzama, South Aït Ahmane and North Aït Ahmane, respectively, Fig. 10d).

5.3.2. Trace element

Serpentinites from the three units display low to very low incompatible element concentrations such as Ti (3.52 to 64.25 ppm; Fig. 11a), REE (rare earth element, ΣREE ranging from 0.045 to 1.38 ppm and Yb from 0.006 to 0.041 ppm, Figs. 11b and 12) and HFSE (e.g. Nb: 0.004–0.099 ppm, Fig. 11).

The serpentinites of the Khzama ophiolitic complex exhibit very low concentrations of incompatible trace elements (e.g., Ti: 14.34–64.25 ppm and Nb: 0.005–0.044 ppm and Yb: 0.009–0.039 ppm, Fig. 11). They are characterized by low REE contents (ΣREE ranging from 0.178 to 0.686 ppm, Fig. 12a) and slightly concave, U-shaped, REE pattern, showing slightly higher LREE (light rare earth elements) and HREE (heavy rare earth elements) compared to MREE (medium rare earth elements) (Fig. 12a). A slight positive anomaly in Eu ($Eu/Eu^* = 1.13$–7.22 times the chondrite) is generally observed for these serpentinites (Fig. 12a). Extended trace element concentrations normalized to the primitive mantle reveal a very weak fractionation between LREE and HFSE, i.e. concentrations of HFSE (high field strength elements, Nb, Ta, Zr, Hf) are close to those of the neighboring REEs (La/Nb and Nd/Zr, respectively between 1.08–18.64 and 0.43–6.43 times the values of the primitive mantle) (Fig. 12b). Multi-elemental spidergrams are rather flat, besides a strong positive anomaly in Pb (Pb/Ce ratio between 6.80 and 7290 × PM) and another one, more variable and moderate, in U (U/Th between 2.77 and 157 × PM, Fig. 12b).

The serpentinites of the South Aït Ahmane Unit are characterized by very low contents in incompatible trace elements (e.g., Ti: 3.52–41.70 ppm, Nb: 0.004–0.077 ppm and Yb: 0.006–0.040 ppm, Fig. 11) similar to the Khzama serpentinites. They show low and more variable REE concentrations relative to the Khzama ones (ΣREE = 0.045–0.693 ppm, Fig. 12c). They also present slightly concave (U-shaped) REE spectra, except for one sample showing important L-MREE enrichment and for two others showing important LREE and variable Eu enrichments (Fig. 12c), similar to these reported by

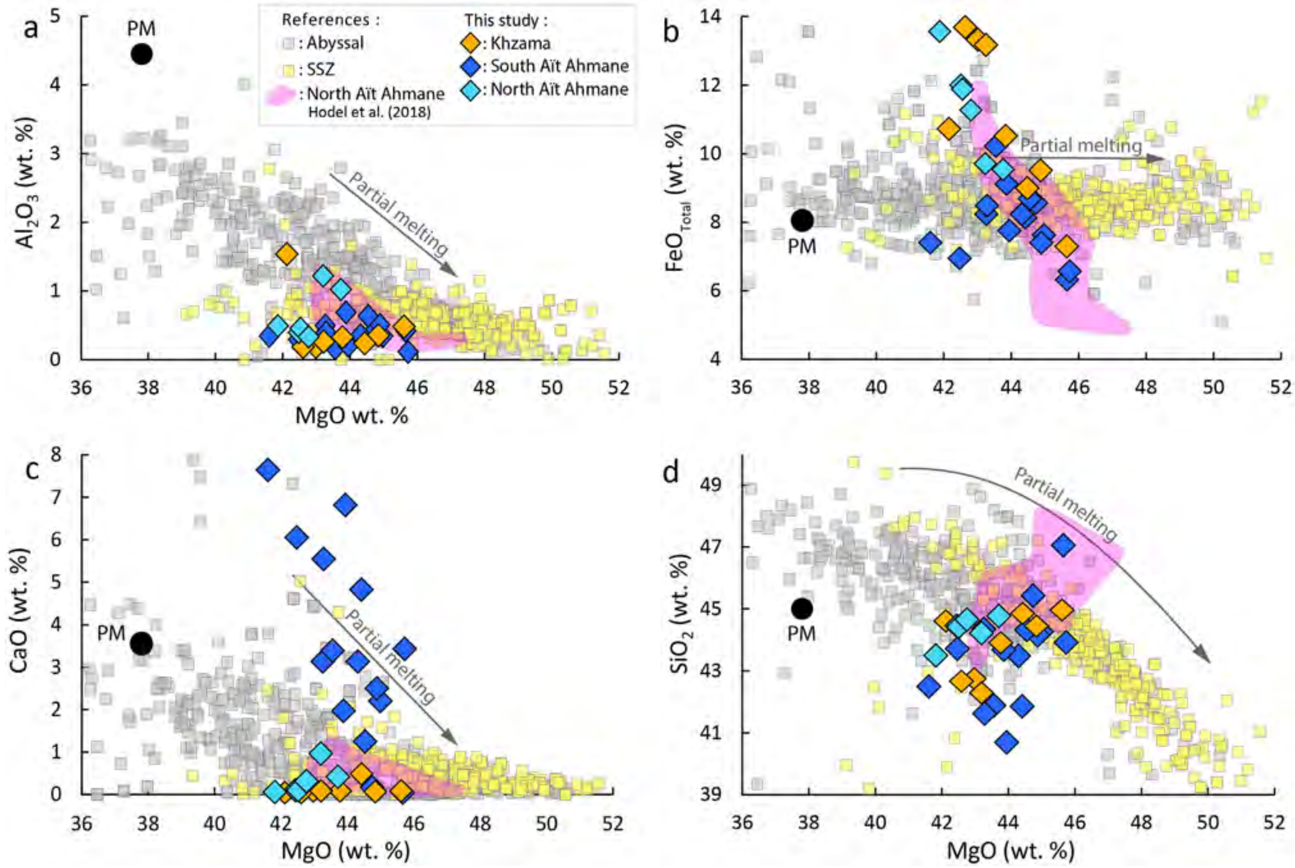

Fig. 10. Bulk-rock major oxides contents vs. MgO content (wt%) diagrams for the Khzama and Aït Ahmane (South and North) serpentinites. Element concentrations are recalculated on a LOI-free basis. (a) Al2O3 vs. MgO; (b) FeO vs. MgO, (c) CaO vs. MgO and (d) SiO2 vs. MgO contents. The pink domain corresponds to the North Aït Ahmane variously hydrothermalized serpentinites of the Hodel et al. (2018) study. Data for abyssal peridotites are from Snow and Dick (1995), Casey (1997), Niu (2004), Paulick et al. (2006), Godard et al. (2008), Augustin et al. (2012), Boschi et al. (2013), Andreani et al. (2014), Chen et al. (2015). Data for SSZ peridotites are from Ishii et al. (1992), Parkinson and Pearce (1998), Pearce et al. (2000), Savov et al. (2005, 2007), Marchesi et al. (2006, 2009), Kodolányi et al. (2012). Primitive Mantle (PM) values are from McDonough and Sun (1995). (For interpretation of the references to colour in this figure legend, the reader is referred to the web version of this article.)

Hodel et al. (2018) for hydrothermalized serpentinites from the North unit. Apart from these two last samples, extended trace element concentrations normalized to the primitive mantle reveal a very weak fractionation between LREE and HSFE (Figs. 12d and 14), as evidenced by the low La/Nb and Nd/Zr ratios, respectively comprised between 0.64 and 6.33 and 0.85–16.78 × PM (Fig. 12d).

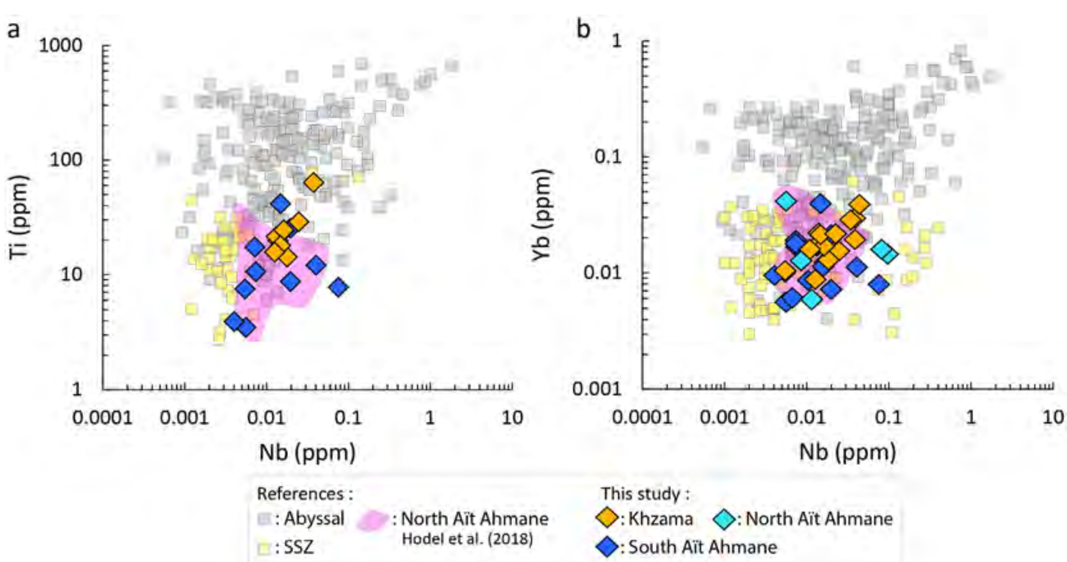

Fig. 11. Plot of the whole-rock (a) Ti vs. Nb and (b) Yb vs. Nb contents for the Khzama and Ahmane serpentinites. The pink domain corresponds to the North Aït Ahmane variously hydrothermalized serpentinites of the Hodel et al. (2018) study. References for the compiled data from abyssal and SSZ peridotites and serpentinites are the same as for the Fig. 10. (For interpretation of the references to colour in this figure legend, the reader is referred to the web version of this article.)

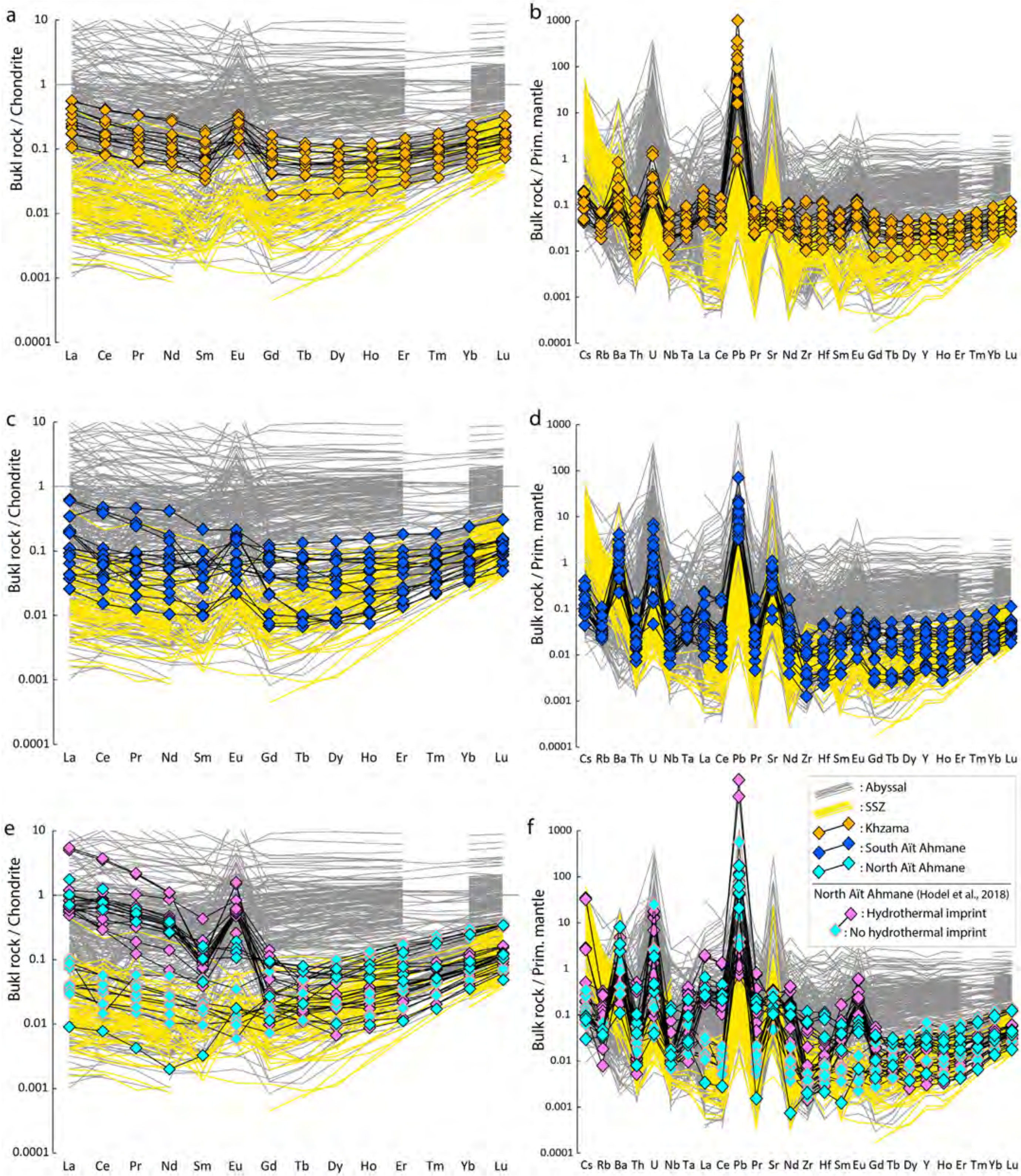

Fig. 12. (a, c, e) Chondrite-normalized REE patterns of the Khzama and of the Aït Ahmane serpentinites. Chondrite values are from Barrat et al. (2012). (b, d, f) Primitive mantle-normalized multi-element patterns of the Khzama and the Aït Ahmane serpentinites. Primitive mantle values are from McDonough and Sun (1995). Data for abyssal peridotites and serpentinites are from Niu (2004), Paulick et al. (2006), Godard et al. (2008), Augustin et al. (2012), Boschi et al. (2013), Andreani et al. (2014), Chen et al. (2015). Data for SSZ peridotites and serpentinites are from Parkinson and Pearce (1998), Pearce et al. (2000), Savov et al. (2005, 2007) and Kodolányi et al. (2012).

Samples AH03 and L53 with marked LREE enrichments show La/Nb and Nd/Zr ratios of 26.46 and 13.07 × PM and of 21.4 and 22.4 × PM, respectively. Similar to the Khzama serpentinites, the South Aït Ahmane serpentinites are notably enriched in Ba (Ba/Th ratios between 12.34 and 446 × PM), in U (U/Th between 1.92 and 516 × PM), in Pb (Pb/Ce ratio between 56.93 and 3637 × PM)

(Fig. 12d). These samples also display a marked positive anomaly in Sr (Sr/Nd ratio between 0.59 and 121 × PM; Fig. 12d).

The samples collected in the North Aït Ahmane unit attest of the geochemical heterogeneity of the serpentinites from this unit. They are also characterized by low to very low incompatible trace elements contents (e.g. Nb: 0.006–0.099 ppm and Yb: 0.006–0.041 ppm, Fig. 11) and variable REE contents (ΣREE = 0.11–1.38 ppm, Fig. 12e). Based on HREE, we distinguish two types of serpentinite protolith, also noticeable in the previous sampling of Hodel et al. (2018) (Fig. 12e): (1) concave patterns and very low HREE contents and (2) convex patterns showing higher HREE concentrations. Based on LREE patterns, several subsets are identified (Fig. 11e): Sample L37 display a strongly LREE-depleted spoon-shaped REE pattern (ΣREE = 0.11 ppm, Fig. 12c), with convex HREE pattern similar to those noticed above. Inversely, sample L34A shows the same REE element pattern than the serpentinites belonging to the nearby fossil hydrothermal system described by Hodel et al. (2018), i.e. a strong LREE enrichment (La/Yb ratio of 50.87 times the chondrite) and a marked positive Eu anomaly (Eu/Eu* = 5.38 times the chondrite) (Fig. 12e). For this sample, high La/Nb of 37.44 times the primitive mantle values suggest that hydrothermal processes likely led to amagmatic LREE enrichment (e.g., Hodel et al., 2018, Fig. 12f, see further discussion). Finally, the samples L32, L34B and L36 display important enrichments in L-MREE and flatter REE patterns (Fig. 12f).

6. In situ U-Pb dating

Zircons and apatites were extracted from the metagabbroic unit of the Northern Aït Ahmane ophiolitic unit (sample L72: UTM29N-WGS84: X 731998 m – Y 3373222 m). Sample L72 consists of a layered metagabbro exposed as a pluri-metric tectonic slice intercalated within the serpentinite units (see location on Fig. 2b). It is part of the type *1*, N-MORB-like metagabbro previously described (see Fig. 8). Zircon and apatite crystals were extracted via heavy liquid (Methylene Iodide), magnetic separation and manual hand-picking. Optical cathodoluminescence images (CL, see Appendix A1 for imaging conditions) were captured to select the location of the spots for LA-ICP-MS analyses (see Appendix A1 for analytical methods and procedure). The full U-Pb isotopic dataset and calculated ages can be found in Supplementary material 6. Concordia diagrams and calculated ages have been produced using IsoplotR (Vermeesch, 2018).

6.1. Zircon U-Pb age

Zircon grains are 50 to 120 μm long, prismatic and colorless showing euhedral to subhedral shape with rounded edges. They are relatively homogeneous in terms of luminescence. They show occasional oscillatory zoning (Fig. 13b) suggesting magmatic crystallization (Corfu et al., 2003). They do not show any evidence for inheritance from older cores. This magmatic origin is confirmed by the high Th/U ratios with an average value of 0.23 in contrast with low Th/U ratios attributed to metamorphic zircons (e.g., Hoskin and Schaltegger, 2003). Their general low contents in U and Th (hence, Pb) are consistent with crystallization in a mafic magma (Kydonakis et al., 2014). The isotopic data plot in a concordant to discordant position in a Tera-Wasserburg concordia diagram (Fig. 13a), due to the presence of variable amounts of common Pb within the zircon grains. They define a lower intercept date of 745.9 ± 7.4 Ma (MSWD = 1.3, n = 32). We refined these data by selecting U-Pb analyses showing more 95% of concordance (n = 15). Plotted in a Wetherill Concordia diagram, these data yield a well-constrained concordant age of 758.7 ± 2.1 Ma (MSWD = 0.75).

6.2. Apatite U-Pb age

Apatites are 40 to 90 μm long and colorless showing subhedral shape with rounded edges. They show a homogeneous luminescence pattern (Fig. 13d). Under the microscope, apatite typically occurs at grain joints between amphibole and plagioclase (Fig. 3a). The 2-sigma ellipses are widely spread (MSWD = 3, n = 30, Fig. 13c). Uncorrected isotopic data are aligned in Tera-Wasserburg diagram yielding a lower intercept date of 659 ± 7 Ma (Fig. 13c).

7. Discussion

7.1. Regional significance of the Aït Ahmane ophiolite U-Pb zircon and apatite ages

The age of the Anti-Atlas ophiolitic complexes and by extension, of the Neoproterozoic oceanic spreading that precedes the Pan-African orogeny in the Anti-Atlas, has been debated in the past. The Sirwa ophiolite has been dated at 762 ± 2 Ma using U-Pb method on zircon grains from a plagiogranite (Samson et al., 2004). Concerning the Bou Azzer ophiolite, the first proposed age for the oceanic crust was determined ca. 788 ± 10 Ma (Clauer, 1976) using Rb-Sr method on sedimentary sequence in direct contact with intrusive mafic rocks from the ophiolitic sequence, and therefore, interpreted as metamorphic age due to the emplacement of the mafic magmatic rocks. El Hadi et al. (2010) dated metagabbroic units at 697 ± 8 Ma (U-Pb on zircons) and interpreted this date as the age of the Bou Azzer ophiolite. These ones are exposed in the Bougmane complex located to the southern part of the Bou Azzer inlier and disconnected from the ophiolitic units. Moreover, Triantafyllou et al. (2018) dated similar metagabbroic rock associated to mafic granulite in the Bougmane complex at 706 ± 9 Ma. These authors showed that they were formed in the lower crust of a thick oceanic arc and that they are consequently not directly related to the evolution of the SSZ spreading system. Hence, this metagabbroic rock do not belong the Bou Azzer ophiolite.

Our study provides a U-Pb age for the Aït Ahmane sequence obtained on zircon from a layered metagabbro, which provides an age at 759 ± 2 Ma (Fig. 13a). This metagabbro is part of the ophiolitic sequence (Fig. 2b) as attested by its NMORB chemical signature (also showing LILE enrichment, Fig. 8), its structural position between metabasalts and serpentinites and the absence of granulite-grade recrystallization. We interpret this date as the crystallization age for this metagabbro protolith. This new age is in agreement with previous Rb-Sr dating (Clauer, 1976). It thus constitutes the best estimate of the age of the Bou Azzer ophiolite.

Our study also provides a U-Pb date of 659 ± 7 Ma for apatite grains extracted from the same layered metagabbro (sample L72, Fig. 13c). As apatite closure temperature for Pb diffusion is low (375–550 °C), U-Pb ages from apatite can be interpreted as cooling ages and/or resetting during a thermal event (e.g. Cherniak et al., 1991; Chamberlain and Bowring, 2001; Schoene and Bowring, 2007; Cochrane et al., 2014). Hence, this age could be interpreted: (i) as a reset of the U-Pb isotopic chronometer during the 650–660 Ma arc magmatic pulse marked in the area by the emplacement of numerous dioritic intrusions within the ophiolitic sequence; or (ii) as the early retrograde stage following the amphibolitisation of these ophiolitic gabbroic units. 659 Ma closely corresponding to the age of intrusive diorites into the Bou Azzer ophiolitic sequence, we suggest that this age represents thermal resetting of the apatite in the metagabbro during the last magmatic pulse affecting the Anti-Atlasic supra-subduction system (Triantafyllou et al., 2020).

These new ages suggest that both Bou Azzer and Sirwa ophiolites were formed during the same oceanic spreading event between 760 and 730 Ma, concurrently with the first built-up stage of an intra-oceanic arc recorded in Tachakoucht, Tazigzaout, Bougmane complexes (with oldest magmatic ages constrained at 743 Ma, 753 Ma and 755 Ma; e.g. Thomas et al., 2002; D'Lemos et al., 2006; Admou et al., 2013).

7.2. Magma heterogeneities representative of back-arc magmatism

After describing the Bou Azzer (Leblanc, 1975) and the Sirwa (Chabane, 1991) sequences as oceanic lithosphere remnants, previous

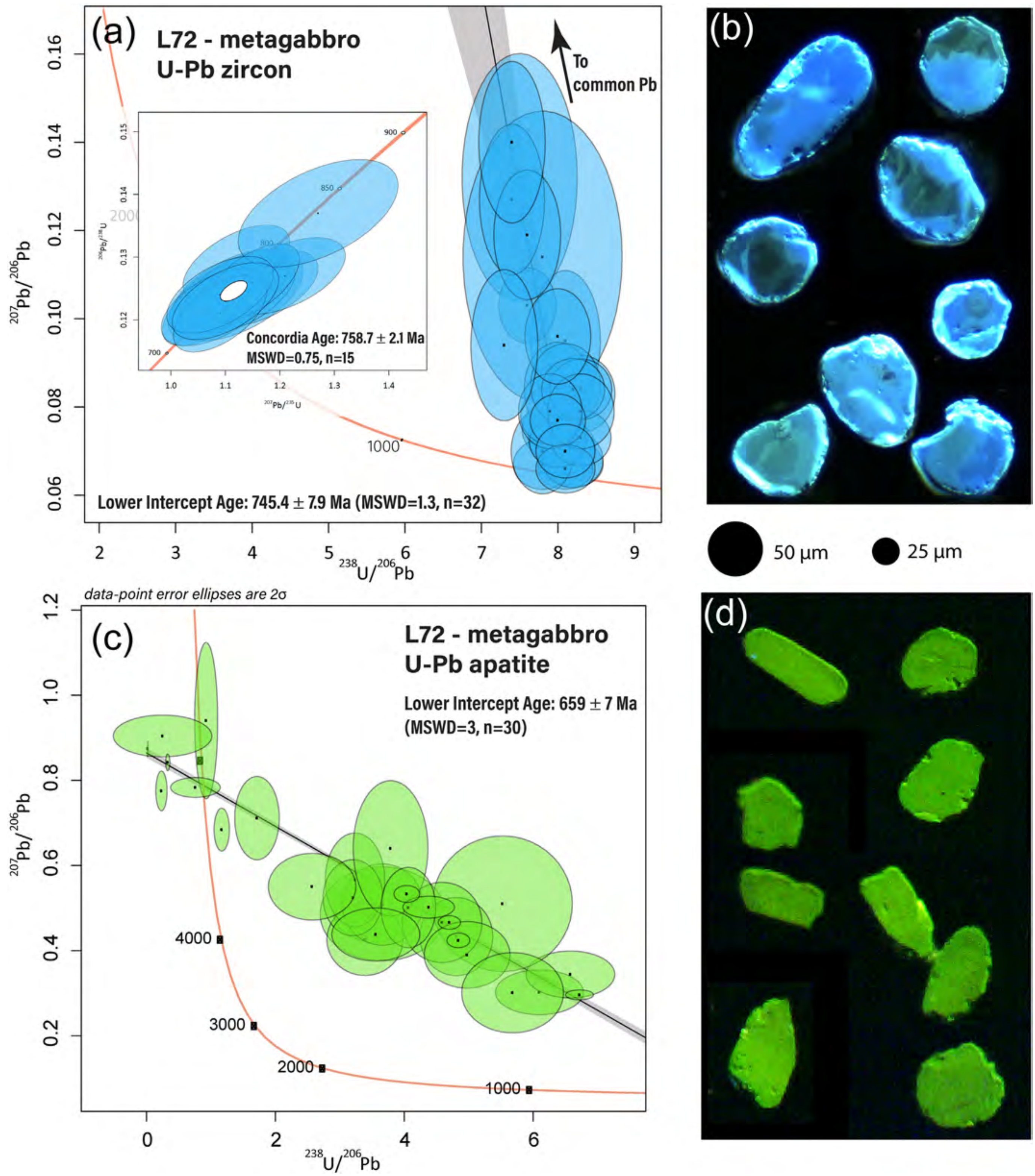

Fig. 13. (a) Tera–Wasserburg and Wetherill Concordia (embedded) U-Pb diagram for zircons extracted from L72 metagabbro. The latter yields a concordant age at 758.7 ± 2.1 Ma (MSWD = 0.75). (b) Optical CL (cathodoluminescence) microphotographs of analyzed zircons. (c) Tera–Wasserburg U-Pb diagram for apatites extracted from L72 metagabbro. Lower intercept yields an age at 659 ± 7 Ma (MSWD = 3). (d) Optical CL microphotographs of the analyzed apatite grains.

studies suggested on the basis of the composition of mafic lavas that these ophiolitic sequences were related to the Anti-Atlasic subduction zone bordering the WAC and associated volcanic arcs (e.g., Naidoo et al., 1991; Bodinier et al., 1984; Triantafyllou et al., 2016, 2018, 2020). Field observations and magnetic geophysical survey (Soulaimani et al., 2006; Hefferan et al., 2014; Triantafyllou et al., 2016, 2018, 2020) demonstrated that the main structures accommodating the Cryogenian ophiolite and arc accretions are dipping to the north with a southward vergence. Accordingly, from a geometrical point of view, the arc complexes being located to the south of the dismembered ophiolite, the latter consequently represents the back-arc domain (Fig. 2a, b). In parallel, fore-arc basalt such as those from the Izu-Bonin system are extremely homogeneous, depleted in incompatible trace-elements compared to MORBs and are characterized by very low Th/Yb and Nb/Yb ratios (Reagan et al., 2010; Hickey-Vargas et al., 2018). They usually alternate with boninitic lavas having basic to intermediate SiO_2 contents (typically 50–60 wt%) with elevated MgO (>10 wt%) (Reagan et al., 2017; Woelki et al., 2018). Such geochemical signatures have not been found in the Anti-Atlas ophiolites, supporting the idea that they originate from a back-arc setting.

As a whole, the geochemical signatures of mafic rocks from the Aït Ahmane and Khzama ophiolitic sequences are heterogeneous, in line with the magma heterogeneity that characterize back-arc environments (e.g., Shinjo et al., 1999; Taylor and Martinez, 2003; Pearce et al., 2005; Tian et al., 2008; Bézos et al., 2009). Indeed, geochemical heterogeneity is one the hallmarks of BABB (Back-Arc Basin Basalts) due to their inherited MOR-like signature coupled with variable amount of subduction component imprint (e.g. Pearce et al., 2005; Pearce and Stern, 2006). The parental magmas of metabasalts from the Anti-Atlas ophiolites appear to have been variously impacted by subduction related processes. They show geochemical signatures ranging from LREE depleted to LREE enriched composition, which are always accompanied by a negative Nb anomaly (Fig. 6). They also display various incompatible element abundances such as Ti and Zr (Ti/Yb and Zr/Yb ranging from 1208 to 4227 and 11–56 respectively), which when high fall in the MORB array and when low sign a SSZ setting (Fig. 7b, c). Finally, they also show LILE enrichments (Fig. 6) and high and variable Th/Yb ratios (0.06–1.07) for quite low Nb/Yb (0.60–3.41) compared to MORBs, reflecting that up to 4% of a slab-derived component enriched their mantle source (Fig. 7). Regarding metagabbros, in Aït Ahmane, some trace-element rich metagabbros display N-MORB fingerprints similar to upper crust gabbroic rocks of the Samail ophiolite, while others are much more depleted similarly to lower gabbros of the Samail ophiolite (Fig. 8). This likely reflects magmatic differentiation processes. These metagabbros can therefore derive similarly from upper and lower crust section in Aït Ahmane. In either case, they are characterized by low Th/Yb ratios (0.01–0.04), which suggest a depleted mantle decompression melting without major subduction component. Such MORB-like magmas devoid of Nb-Ta anomalies, i.e. not influenced by subduction components, are common in back-arc domains worldwide (Taylor and Martinez, 2003; Pearce et al., 2005).

Hence, this geochemical heterogeneity of mafic lithologies and the association of both MORB-like and subduction related melts tend to confirm that the Khzama and Aït Ahmane oceanic lithosphere were formed in a back-arc environment (e.g. Shinjo et al., 1999; Taylor and Martinez, 2003; Pearce et al., 2005; Tian et al., 2008).

7.3. Origin of the variably depleted signature of the Anti-Atlas serpentinites

Ultramafic units of the Moroccan Anti-Atlas ophiolites remain poorly constrained in terms of geochemistry. Through this study, we challenged to study the geochemical signature of serpentinites in order to decipher their primary chemical signal, and thus to constrain the magmatic history of these mantle rocks.

7.3.1. Serpentinization imprint and exclusion of hydrothermalized samples

Given this petrogenetic purpose, a sorting was necessary to dissociate magmatic vs. hydrothermal geochemical imprints in order to discard samples for which pristine magmatic signature is not well preserved.

It has been shown that LREE and, in a lesser extent, MREE (particularly Eu) can be strongly affected – enriched relatively to HREE – by hydrothermal processes involving hot acidic fluids, as those encountered in black smoker type hydrothermal systems for instance (e.g. Paulick et al., 2006; Craddock et al., 2010; Andreani et al., 2014; Hodel et al., 2018). However, LREE and MREE enrichments in depleted ultramafic rocks also often result of melt-rock reaction or refertilization processes before serpentinization (e.g. Navon and Stolper, 1987; Vernières et al., 1997; Godard et al., 2000, 2008; Bodinier and Godard, 2003; Saka et al., 2014; Warren, 2016). A relevant way to discriminate a magmatic or hydrothermal origin for L-MREE enrichments in serpentinized peridotites is to consider their HFSE contents. Indeed, these latter are not – or very slightly – mobilized during serpentinization and hydrothermal processes (You et al., 1996; Kogiso et al., 1997; Niu, 2004; Paulick et al., 2006; Deschamps et al., 2013). Thus an important fractionation between LREE and HFSE signs a hydrothermal (i.e. aqueous) imprint, while unfractionated HFSE and LREE contents reflect magmatic processes involvement (e.g. Niu, 2004; Paulick et al., 2006, Hodel et al., 2018; Fig. 14).

Hodel et al. (2018) previously shown that most of the serpentinites of the North Aït Ahmane unit displayed important LREE enrichments and strong LREE vs. HFSE fractionation (Figs. 12 and 14), as a result of intense hydrothermal alteration. Two other serpentinite samples from the North Aït Ahmane unit (samples L34A and L36) display similar geochemical signature, attesting a potential link with this episode. Other serpentinites from the South Aït Ahmane unit (samples AH01B, AH03, L50 and L53) and from the Khzama unit (sample SH09 and KK14A) also show LREE enrichments and important LREE vs. HFSE fractionation reflecting a probable hydrothermal origin for these signatures as well (Fig. 14). Setting aside these samples, L-MREE enrichments noticed for most of the Khzama and the Aït Ahmane serpentinites studied here (U-shaped REE patterns, Fig. 12a, c, e) are almost always accompanied by HFSE enrichment testifying of their magmatic origin (Figs. 12 and 14). We therefore excluded all the samples showing hydrothermal

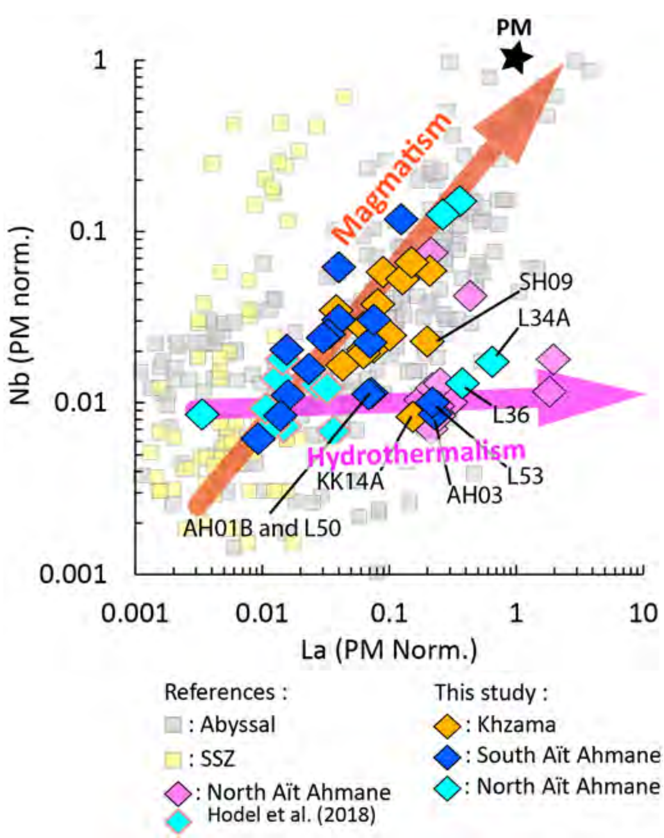

Fig. 14. Primitive Mantle (PM) normalized Nb vs La contents of the Khzama and the Aït Ahmane serpentinites allowing deciphering between hydrothermal and magmatic processes to explain LREE enrichments in most of the serpentinites from the three units (U-shaped REE patterns, Fig. 12a, c, e). Legend for the North Aït Ahmane serpentinites analyzed by Hodel et al. (2018) is the same as in Fig. 12. Primitive mantle values are from McDonough and Sun (1995). Compilation used for abyssal and SSZ peridotites and serpentinites is the same as for previous figures.

geochemical imprint of our following magmatic investigations (samples L34A, L36, AH01B, AH03, L50, L53, SH09 and KK14A).

7.3.2. Multiple stages of mantle partial melting and liquid extraction

Both Khzama and Aït Ahmane serpentinites show very low Al_2O_3 contents (Figs. 9 and 10), together with intermediate to high spinels' Cr# and low to high Mg# ratios (Fig. 5a) suggesting a highly depleted ultramafic protolith. These proxies attest of a partial melting ranging from 25% to more than 35% for the precursor of the Khzama and Aït Ahmane serpentinites (Fig. 5a). Such extreme melting degrees are not compatible with MOR-like dry decompression melting (e.g., Dick and Bullen, 1984; Ishii et al., 1992; Arai, 1994; Warren, 2016). They are nowadays considered as being one of the hallmarks of the supra-subduction environments, where peridotites experience intense and/or multiple flux melting episodes (Bizimis et al., 2000; Barth et al., 2008; Ulrich et al., 2010; Uysal et al., 2012, 2016). Low incompatible trace elements (Ti, Nd and Yb) and REE contents also fit with these commonly reported for SSZ fresh and serpentinized peridotites (Figs. 11 and 12).

To better constrain partial melting and fluid-melt-rock interaction processes, we performed partial melting modelling using REE compositions of the serpentinites via closed- and open-dynamic melting reactions (see equilibrium equations reviewed in Zou, 2007) (Fig. 15). These melting models are non-modal dynamic melting. Porosity value (φ) has been set to 1% and corresponds to the proportion of melt trapped in the residue composition (e.g. Uysal et al., 2012). Starting mantle composition is DMM (Depleted MORB Mantle; after Workman and Hart, 2005), which reproduces typical compositional range of depleted peridotite composition formed in abyssal context (see Fig. 11 in the review paper of Warren, 2016) after 10–17% of partial melting of non-depleted Primitive Mantle (PM) (e.g., Uysal et al., 2016; Hao et al., 2016). Models' parameters and partition coefficients are presented in Supplementary material 7.

Here we used HREE (Yb, Lu) concentrations to constrain partial melting degree for the studied serpentinites; MREE and LREE being strongly affected by metasomatism and magmatic refertilization processes (modal and cryptic, Navon and Stolper, 1987; Godard et al., 1995; Vernières et al., 1997; Warren and Shimizu, 2010). Based on HREE abundances, two groups have therefore been identified (group A and group B, respectively marked by high and low HREE; Fig. 15). Group A serpentinites result of F: 15% partial melting in a closed dynamic model (see gray lines in Fig. 15a) while group B serpentinites are residues after higher partial melting degree (F: 18–19%; Fig. 15b, c). The group B could be divided in two subgroups, B1 and B2, based on HREE contents. Group B1 REE patterns are well clustered, while HREE from B2 group serpentinites show more spread values, probably due to the slight influence of melt-rock interaction discussed in the next section.

This variability in partial melting degree along with the highly depleted character of the Khzama and Aït Ahmane serpentinites attests of their complex magmatic history. They both suggest that these residues were affected by at least two partial melting events. For both scenarios, high degrees of partial melting (sum of F of two melting episodes ranging between: 20 and 33%) are in agreement with those recorded by spinel composition (Fig. 5) and major elements bulk-rock composition (Figs. 9 and 10).

7.3.3. Interaction between SSZ fluid-melt-mantle rocks

Most of the studied serpentinites show enrichments in LREE and/or in MREE contents that are not predicted by classic closed system melt-

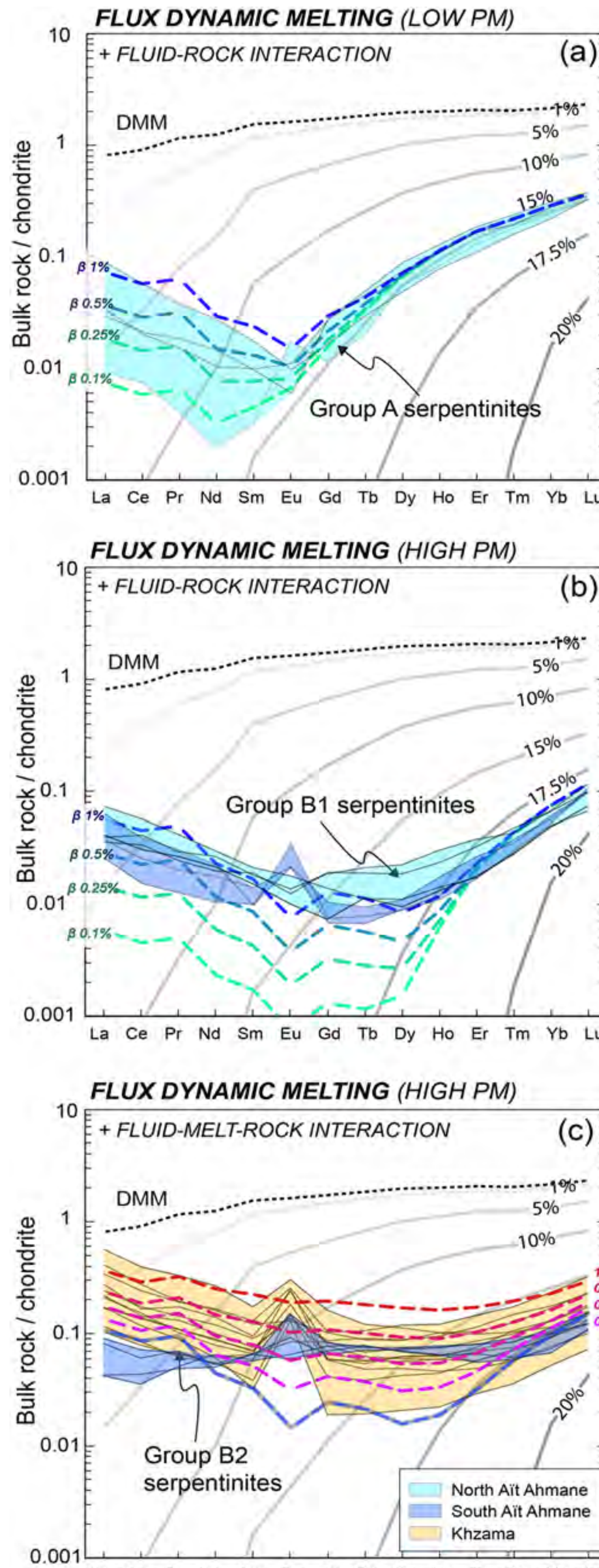

Fig. 15. Closed- and open-dynamic melting model of a Depleted MORB Mantle (DMM) protolith. Modelled patterns are compared to REE composition of Aït Ahmane and Khzama serpentinites. Black dashed line is for DMM starting composition (after Workman and Hart, 2005). Gray lines in (a), (b) and (c) are for closed-system non-modal dynamic melting (porosity φ = 1%). Green to blue lines in (a) and (b) are for open-system non-modal dynamic melting (φ = 1% and SSZ-fluid influx β from 0.1 to 1% after Eiler et al., 2000, 2007). Pink to red lines in (c) are for melt-rock mixing model between a flux molten residue and an IAB (X from 0.1 to 1%). See Sections 7.3.2 and 7.3.3 and Supplementary material 7 for more details about the model's parameters. (For interpretation of the references to colour in this figure legend, the reader is referred to the web version of this article.)

ing models (Vernières et al., 1997; Godard et al., 2000, 2008; Bodinier and Godard, 2003 and see gray lines in Fig. 15). LREE-MREE enrichments producing the U-shaped REE patterns of the Khzama and the Aït Ahmane being, in most cases, accompanied by HFSE enrichments (Fig. 14), they likely originate from magmatic (refertilization/enrichment) processes in an open system. Similar concave REE patterns are commonly reported for heavily depleted peridotites and ophiolitic serpentinites from subduction contexts and are interpreted as resulting of intense and/or multiple hydrous partial melting associated with refertilization or metasomatic processes involving subduction related LREE-rich melts (Prinzhofer and Allègre, 1985; Gruau et al., 1998; Dubois-Cote et al., 2005; Barth et al., 2008; Ulrich et al., 2010; Uysal et al., 2012, 2015, 2016). In addition, high Ti content (up to 0.26 wt% TiO_2, Fig. 5b) in spinels from the Khzama serpentinite comforts post/*syn*-melting melt-rock interaction involving melts derived from the subduction system, as commonly observed for peridotites in supra-subduction (SSZ) environment (e.g., Bizimis et al., 2000; Pearce et al., 2000; Ulrich et al., 2010; Uysal et al., 2015, 2016) (Fig. 5b). Such melt/rock interaction processes are also corroborated by the REE patterns of these Khzama serpentinites, which display the strongest LREE-MREE enriched, U-shaped REE patterns (see modelling approach below).

To reproduce LREE and MREE signature, we also performed open-system dynamic melting model with the same parameters described in Section 7.3.2. We used DMM as protolithic composition too but using a subduction component (SSZ-fluid gathered and compiled from Eiler et al., 2000, 2007) as influx material quantified by the parameter β (expressed in %; see green to blue lines in Fig. 15a, b). The group A1 serpentinites (North Aït Ahmane unit only) show a convex HREE pattern and a strong bend of MREE to LREE pattern (centered on Eu; Fig. 15a). This group is well modelled using such a flux dynamic melting (Fig. 15a) with melting degree comprises between 15 and 16% and variable SSZ-fluid influx value (β) ranging from 0.1 to 1.0%. The group B1 (North and South Aït Ahmane) and B2 (South Aït Ahmane and Khzama) serpentinites are marked by a smoother and concave HREE pattern resulting from a REE enrichment affecting both L- and MREE (and even HREE for Khzama samples) (Fig. 15c). For the B1 group serpentinites, dynamic melting model predicts a higher partial melting degree ranging from 18 to 19% and similar influx β value of 0.5 to 1.0%. Nonetheless, for some samples, higher content in MREE to HREE (Gd to Er) relative to the fluid-only dynamic model could be better explained by a slight interaction with a melt as shown in Fig. 15c. The B2 group serpentinites are well modelled using a flux dynamic melting (Fig. 15c), with high melting degree and moderate proportions of subduction component influx similar to B1 group (F: 19% and β: 0.5–1.0%, see blue dashed line on Fig. 15c) subsequently affected by melt-rock interactions with 0.1 to 1.0% (parameter X) of percolating arc-related basalts (see pink to red dashed lines on Fig. 15c; we here used a median of IAB gathered from PetDB; in Supplementary material 7). We also compared with averaged boninitic and BABB available but IAB composition fit better. Group B2 serpentinites composition could thus be reasonably explained by a combination of subduction influx during the melting event and by subsequent melt-rock interactions with percolating arc related basalts, as recorded by high Ti contents of the Khzama serpentinites spinels and moderate values for the other serpentinite samples (Fig. 5b).

7.4. Conclusions

- Our new geochronological data confirms the petrogenetic link between the Sirwa (762 ± 2 Ma, Samson et al., 2004) and the Bou Azzer ophiolites (759 ± 2 Ma, this study). These ophiolites probably represent different relics of a same oceanic lithospheric plate, formed

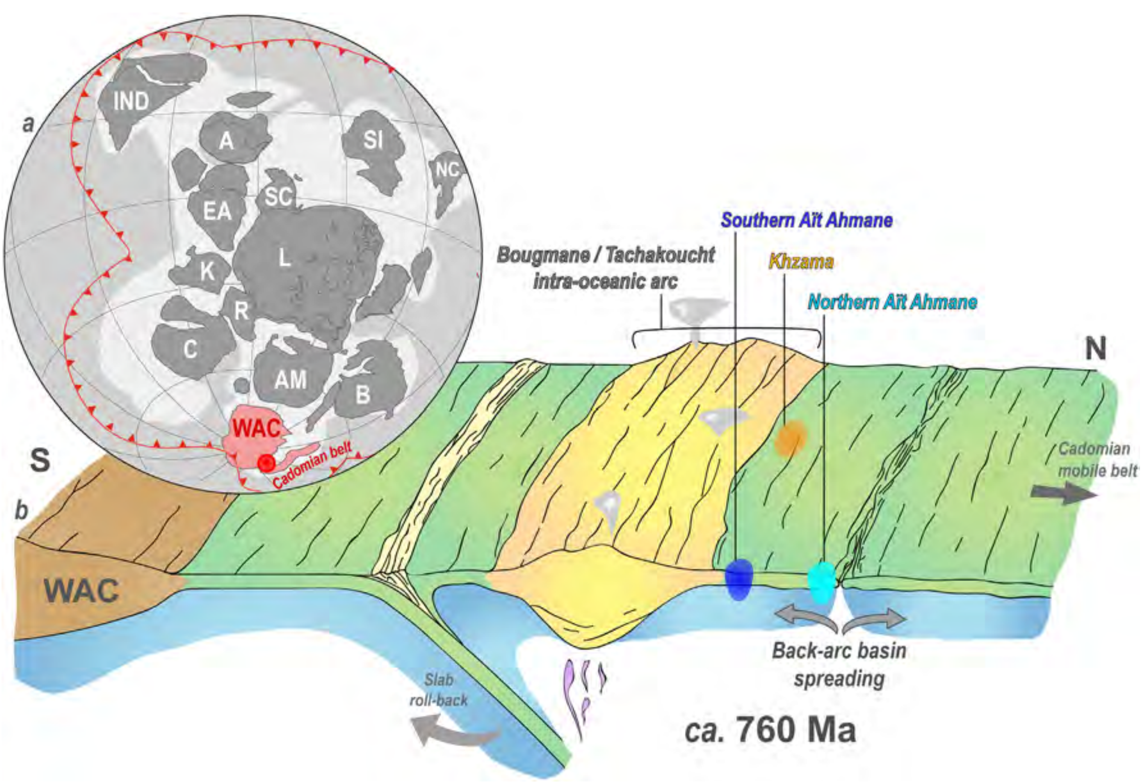

Fig. 16. (a) Earth's paleogeography ca. 780 Ma, while Rodinia initiates its break-up (after Li et al., 2008). The WAC and the associated Cadomian mobile belt southward were located near the South Pole. Red dot represents the approximate location of the Anti-Atlasic subduction zone. Abbreviations are for: IND: India; A: Australia; SI: Siberia; NC: North China; SC: South China; EA: East Antarctica; L: Laurentia; K: Kalahari; R: Rio de la Plata; C: Congo; AM: Amazonia; B: Baltica; WAC: West African Craton. (b) Schematic geodynamic model that we propose for the Anti-Atlas ophiolites genesis, i.e. an intra-oceanic back-arc basin. Khzama and Southern Aït Ahmane units being more affected by SSZ-melts percolations and being closer to arc remnants, they likely originate from an earlier stage of the back-arc domain development compared to the North Aït Ahmane unit. (For interpretation of the references to colour in this figure legend, the reader is referred to the web version of this article.)

synchronously with the first building stage of the Moroccan Anti-Atlas intra-oceanic-arc.

- Considering an ocean-ward subduction geometry, which is nowadays rather consensual, the northern location of the Anti-Atlas ophiolites relative to these arc complexes supports the fact that they formed in a back-arc basin (Fig. 16). The back-arc setting of the three studied ophiolites is also supported by the coexistence of MOR-like and SSZ-related mafic lithologies. Neither boninitic magmatism nor subduction channel melange, nor high to ultra-high pressure-low-temperature relics (which are common in fore-arc domains) have been described so far in the arc-related units in Sirwa and Bou Azzer inliers, discarding their formation in a fore-arc setting.
- Regarding ultramafic rocks, their very low major and trace incompatible element contents, along with high Cr# for low to intermediate Mg# in their constitutive Cr-spinel, denote that these rocks endured high partial melting degrees, which are incompatible (or at least, very uncommon) with dry MOR-like melting. These observations combined to REE melting modelling approach reveal that the Khzama and the Aït Ahmane serpentinites precursor experienced a polyphased open-system melting history, strongly influenced by SSZ-fluid influx and subduction-related melts percolations.
- The variability of the geochemical signatures of mantle rocks between the studied ophiolitic units can be used as a tracer of refertilization intensity, and hence as a marker of vicinity to the sub-arc mantle region (e.g. see Tollstrup et al., 2010's equivalent approach for mafic rocks). Here, the Khzama ophiolitic sequence, is highly affected by SSZ metasomatism and IAB percolation as denoted by Ti-enriched spinels and modelled REE patterns. Similar IAB percolation is also characteristic for the South Aït Ahmane unit but is very uncommon in the North Aït Ahmane ones. In addition, both Khzama and South Aït Ahmane units are geometrically closer to their associated arc complexes (Iriri-Tachakoucht and Bougmane complexes, respectively) compared to the North Aït Ahmane unit. All these observations argue that both Khzama and South Aït Ahmane units were likely formed synchronously during an early spreading stage in the back-arc region. This scenario predicts that their mantle section would be closer to the sub-arc region where intense arc magma production and slab-derived metasomatism prevail. In turn, the northern Aït Ahmane unit likely formed during a later stage of the back-arc spreading, hence being less affected by slab- and sub-arc-derived influxes (Fig. 16).
- Future studies should focus on improving the petrochronological records in each of ophiolitic sequence to testify our geodynamic model and to better constrain the timing and evolution of intra-oceanic arc-back-arc systems.

CRediT authorship contribution statement

F. Hodel: Conceptualization, Investigation, Writing - original draft, Visualization. **A. Triantafyllou:** Conceptualization, Investigation, Funding acquisition, Writing - original draft, Visualization. **J. Berger:** Investigation, Writing - review & editing. **M. Macouin:** Investigation, Supervision, Funding acquisition, Writing - review & editing. **J-M. Baele:** Investigation, Writing - review & editing. **N. Mattielli:** Supervision, Writing - review & editing. **C. Monnier:** Investigation, Supervision, Writing - review & editing. **R.I.F. Trindade:** Supervision, Funding acquisition, Writing - review & editing. **M.N. Ducea:** Supervision, Writing - review & editing. **A. Chatir:** Investigation, Writing - review & editing. **N. Ennih:** Investigation, Supervision, Writing - review & editing. **J. Langlade:** Formal analysis, Validation. **M. Poujol:** Methodology, Formal analysis, Validation, Writing - review & editing.

Declaration of competing interest

The authors declare that they have no known competing financial interests or personal relationships that could have appeared to influence the work reported in this paper.

Acknowledgments

The authors thank O. Bruguier, C. Douchet and L. Causse for their assistance on the ICP-MS and P. De Parseval and M. P. Castro for their assistance on electron microprobes. Authors are also grateful to the Microscopy and Microanalysis Laboratory (LMic) of the *Universidade Federal de Ouro Preto*, a member of the Microscopy and Microanalysis Network of Minas Gerais State/Brazil/FAPEMIG. U-Pb data on zircon were acquired in the GeOHeLiS analytical platform, Rennes University. This work has been funded by Research Grant 2016/06114-6 of the TelluS-SYSTER program of Institut national des sciences de l'Univers (INSU, CNRS, France) and French *Ministère de l'Éducation nationale, de l'Enseignement supérieur et de la Recherche* (MENESR). A.T. thanks the *Rotary Club de Mons* and the University of Mons for providing their financial support via the Pierre Jacobs post-doctoral grant (2018). AT is an FRS-FNRS post-doctoral research fellow for the PROBARC project (Grant CR n°1. B. 414.20F). M.N.D. acknowledges support from US National Science Foundation grant EAR 1725002 and the Romanian Executive Agency for Higher Education, Research, Development and Innovation Funding project PN-III-P4-ID-PCCF-2016-0014. The authors are also grateful to Prof. A. Hassan and an anonymous reviewer for their careful reading and suggestions, which significantly improved this contribution. F.H. and A.T. are both first authors and contributed equally to this work.

Data availability

All data used in this manuscript are available in Supplementary materials 1–9. Further queries and information requests should be directed to the lead authors F.H. (florent.hodel@hotmail.fr) and A.T. (antoinetri@gmail.com).

Appendix A. Supplementary data

Supplementary data associated with this article can be found in the online version, at https://doi.org/10.1016/j.gr.2020.05.014. These data include the Google map of the most important areas described in this article.

References

Admou, H., Juteau, T., 1998. Discovery of a fossil oceanic hydrothermal system in the Late Precambrian Khzama ophiolite (Siroua massif, Anti-Atlas range, Morocco). Comptes Rendus l'Academie des Sci. Ser. IIA Earth Planet. Sci. 5, 335–340.

Admou, H., Razin, P., Egal, E., Youbi, N., Soulaimani, A., Blein, O., Chevremont, P., Gasquet, D., Barbanson, L., Bouabdelli, M., Anzar, C., 2013. Notice explicative de la Carte géologiques du Maroc (1/50 000), feuille Aït Ahmane. Notes Mémoires du Serv. Géologique du Maroc carte.

Ahmed, H., Arai, S., Abdel-Aziz, Y.M., Rahimi, A., 2005. Spinel composition as a petrogenetic indicator of the mantle section in the Neoproterozoic Bou Azzer ophiolite, Anti-Atlas, Morocco. Precambrian Res. 138, 225–234. https://doi.org/10.1016/j.precamres.2005.05.004.

Ahmed, A.H., Arai, S., Ikenne, M., 2009. Mineralogy and paragenesis of the Co-Ni arsenide ores of Bou Azzer, Anti-Atlas, Morocco. Econ. Geol. 104, 249–266. https://doi.org/10.2113/gsecongeo.104.2.249.

Andreani, M., Escartin, J., Delacour, A., Ildefonse, B., Godard, M., Dyment, J., Fallick, A.E., Fouquet, Y., 2014. Tectonic structure, lithology, and hydrothermal signature of the Rainbow massif (Mid-Atlantic Ridge 36°14′N). Geochem. Geophys. Geosyst. 15, 3543–3571. https://doi.org/10.1002/2014GC005269.

Arai, S., 1994. Compositional variation of olivine-chromian spinel in Mg-rich magmas as a guide to their residual spinel peridotites. J. Volcanol. Geotherm. Res. 59, 279–293. https://doi.org/10.1016/0377-0273(94)90083-3.

Augustin, N., Paulick, H., Lackschewitz, K.S., Eisenhauer, A., Garbe-Schönberg, D., Kuhn, T., Botz, R., Schmidt, M., 2012. Alteration at the ultramafic-hosted Logatchev hydrothermal field: constraints from trace element and Sr-O isotope data. Geochem. Geophys. Geosyst. 13. https://doi.org/10.1029/2011GC003903 (n/a-n/a).

Bach, W., Garrido, C.J., Paulick, H., Harvey, J., Rosner, M., 2004. Seawater-peridotite interactions: first insights from ODP Leg 209, MAR 15°N. Geochem. Geophys. Geosyst. 5. https://doi.org/10.1029/2004GC000744 (n/a-n/a).

Barrat, J.A., Zanda, B., Moynier, F., Bollinger, C., Liorzou, C., Bayon, G., 2012. Geochemistry of CI chondrites: major and trace elements, and Cu and Zn isotopes. Geochim. Cosmochim. Acta 83, 79–92. https://doi.org/10.1016/j.gca.2011.12.011.

Barth, M.G., Mason, P.R.D., Davies, G.R., Drury, M.R., 2008. The Othris Ophiolite, Greece: a snapshot of subduction initiation at a mid-ocean ridge. Lithos 100, 234–254. https://doi.org/10.1016/J.LITHOS.2007.06.018.

Bézos, A., Escrig, S., Langmuir, C.H., Michael, P.J., Asimow, P.D., 2009. Origins of chemical diversity of back-arc basin basalts: a segment-scale study of the Eastern Lau Spreading Center. J. Geophys. Res. 114, B06212. https://doi.org/10.1029/2008JB005924.

Bizimis, M., Salters, V.J.M., Bonatti, E., 2000. Trace and REE content of clinopyroxenes from supra-subduction zone peridotites. Implications for melting and enrichment processes in island arcs. Chem. Geol. 165, 67–85. https://doi.org/10.1016/S0009-2541(99)00164-3.

Blein, O., Baudin, T., Chevremont, P., Soulaimani, A., Admou, H., Gasquet, P.A., Cocherie, E., Egal, N., Youbi, f.P., Razin, P., 2014. Geochronological constraints on the polycyclic magmatism in the Bou Azzer-El Graara inlier (Central Anti-Atlas Morocco). J. Afr. Earth Sci. 99, 287–306. https://doi.org/10.1016/J.JAFREARSCI.2014.04.021.

Bodinier, J.-L., Godard, M., 2003. Orogenic, ophiolitic, and abyssal peridotites. Treatise on Geochemistry. Elsevier, pp. 1–73 https://doi.org/10.1016/B0-08-043751-6/02004-1.

Bodinier, J.L., Dupuy, C., Dostal, J., 1984. Geochemistry of Precambrian ophiolites from Bou Azzer, Morocco. Contrib. Mineral. Petrol. 87, 43–50. https://doi.org/10.1007/BF00371401.

Boschi, C., Bonatti, E., Ligi, M., Brunelli, D., Cipriani, A., Dallai, L., D'Orazio, M., Früh-Green, G.L., Tonarini, S., Barnes, J.D., Bedini, R.M., 2013. Serpentinization of mantle peridotites along an uplifted lithospheric section, Mid Atlantic Ridge at 11° N. Lithos 178, 3–23. https://doi.org/10.1016/j.lithos.2013.06.003.

Bousquet, R., El Mamoun, R., Saddiqi, O., Goffé, B., Möller, A., Madi, A., 2008. Mélanges and ophiolites during the Pan-African orogeny: the case of the Bou-Azzer ophiolite suite (Morocco). Geol. Soc. Lond. Spec. Publ. 297, 233–247. https://doi.org/10.1144/SP297.11.

Casey, J.F., 1997. Comparison of major and trace element geochemistry of abyssal peridotites and mafic plutonic rocks with basalts from the mark region of the Mid-Atlantic Ridge. Proc. Ocean Drill. Program Sci. Results 153.

Chabane, A., 1991. Les roches vertes du Protérozoïque Supérieur de Khzama (Siroua, AntiAtlas, Maroc). Un exemple d'ophiolite d'avant arc formé en contexte de faille transformante. Université Cadi Ayyad, Marrakech, Maroc.

Chamberlain, K.R., Bowring, S.A., 2001. Apatite–feldspar U–Pb thermochronometer: a reliable, mid-range (~450°C), diffusion-controlled system. Chem. Geol. 172, 173–200. https://doi.org/10.1016/S0009-2541(00)00242-4.

Chen, L., Chu, F.-Y., Zhu, J.-H., Dong, Y.-H., Yu, X., Li, Z.-G., Tang, L.-M., 2015. Major and trace elements of abyssal peridotites: evidence for melt refertilization beneath the ultraslow-spreading Southwest Indian Ridge (53° E segment). Int. Geol. Rev. 57, 1715–1734. https://doi.org/10.1080/00206814.2015.1029014.

Cherniak, D., Lanford, W., Ryerson, F., 1991. Lead diffusion in apatite and zircon using ion implantation and Rutherford backscattering techniques. Geochim. Cosmochim. Acta 55, 1663–1673. https://doi.org/10.1016/0016-7037(91)90137-T.

Clauer, N., 1976. Géochimie isotopique du Strontium des milieux sédimentaires. Application à la géochronologie de la couverture du Craton Ouest-Africain. Strasbourg.

Cochrane, R., Spikings, R.A., Chew, D., Wotzlaw, J.-F., Chiaradia, M., Tyrrell, S., Schaltegger, U., Van der Lelij, R., 2014. High temperature (>350°C) thermochronology and mechanisms of Pb loss in apatite. Geochim. Cosmochim. Acta 127, 39–56. https://doi.org/10.1016/j.gca.2013.11.028.

Coleman, R.G., Keith, T.E., 1971. A chemical study of serpentinization—Burro Mountain, California. J. Petrol. 12, 311–328. https://doi.org/10.1093/petrology/12.2.311.

Corfu, F., Hanchar, J.M., Hoskin, P.W.O., Kinny, P., 2003. Atlas of zircon textures. Rev. Mineral. Geochem. 53, 469–500. https://doi.org/10.2113/0530469.

Craddock, P.R., Bach, W., Seewald, J.S., Rouxel, O.J., Reeves, E., Tivey, M.K., 2010. Rare earth element abundances in hydrothermal fluids from the Manus Basin, Papua New Guinea: indicators of sub-seafloor hydrothermal processes in back-arc basins. Geochim. Cosmochim. Acta 74, 5494–5513. https://doi.org/10.1016/j.gca.2010.07.003.

Deschamps, F., Godard, M., Guillot, S., Hattori, K., 2013. Geochemistry of subduction zone serpentinites: a review. Lithos 178, 96–127. https://doi.org/10.1016/j.lithos.2013.05.019.

Dick, H.J.B., Bullen, T., 1984. Chromian spinel as a petrogenetic indicator in abyssal and alpine-type peridotites and spatially associated lavas. Contrib. Mineral. Petrol. 86, 54–76. https://doi.org/10.1007/BF00373711.

Dilek, Y., Furnes, H., 2011. Ophiolite genesis and global tectonics: geochemical and tectonic fingerprinting of ancient oceanic lithosphere. Geol. Soc. Am. Bull. 123, 387–411. https://doi.org/10.1130/B30446.1.

D'Lemos, R.S., Inglis, J.D., Samson, S.D., 2006. A newly discovered orogenic event in Morocco: Neoproterozic ages for supposed Eburnean basement of the Bou Azzer inlier, Anti-Atlas Mountains. Precambrian Res. 147, 65–78. https://doi.org/10.1016/j.precamres.2006.02.003.

Dubois-Cote, V., Hebert, R., Dupuis, C., Wang, C., Li, Y., Dostal, J., 2005. Petrological and geochemical evidence for the origin of the Yarlung Zangbo ophiolites, southern Tibet. Chem. Geol. 214, 265–286. https://doi.org/10.1016/J.CHEMGEO.2004.10.004.

Eiler, J.M., Crawford, A., Elliott, T., Farley, K.A., Valley, J.W., Stolper, E.M., 2000. Oxygen isotope geochemistry of oceanic-arc lavas. J. Petrol. 41, 229–256.

Eiler, J.M., Schiano, P., Valley, J.W., Kita, N.T., Stolper, E.M., 2007. Oxygen-isotope and trace element constraints on the origins of silica-rich melts in the subarc mantle. Geochem. Geophys. Geosyst. 8.

El Boukhari, A., Chabane, A., Rocci, G., Tnae, J.L., 1992. Upper Proterozoic ophiolites of the Siroua Massif (Anti-Atlas, Morocco) a marginal sea and transform fault system. J. Afr. Earth Sci. 14, 67–80.

El Hadi, H., Simancas, J.F., Martínez-Poyatos, D., Azor, A., Tahiri, A., Montero, P., Fanning, C.M., Bea, F., González-Lodeiro, F., 2010. Structural and geochronological constraints on the evolution of the Bou Azzer Neoproterozoic ophiolite (Anti-Atlas, Morocco). Precambrian Res. 182, 1–14. https://doi.org/10.1016/j.precamres.2010.06.011.

Furnes, H., Dilek, Y., de Wit, M., 2015. Precambrian greenstone sequences represent different ophiolite types. Gondwana Res. 27, 649–685. https://doi.org/10.1016/j.gr.2013.06.004.

Gahlan, H.A., Arai, S., Ahmed, A.H., Ishida, Y., Abdel-Aziz, Y.M., Rahimi, A., 2006. Origin of magnetite veins in serpentinite from the Late Proterozoic Bou-Azzer ophiolite, Anti-Atlas, Morocco: an implication for mobility of iron during serpentinization. J. Afr. Earth Sci. 46, 318–330. https://doi.org/10.1016/j.jafrearsci.2006.06.003.

Gasquet, D., Levresse, G., Cheilletz, A., Azizi-Samir, M.R., Mouttaqi, A., 2005. Contribution to a geodynamic reconstruction of the Anti-Atlas (Morocco) during Pan-African times with the emphasis on inversion tectonics and metallogenic activity at the Precambrian–Cambrian transition. Precambrian Res. 140, 157–182. https://doi.org/10.1016/j.precamres.2005.06.009.

Gasquet, D., Ennih, N., Liégeois, J.-P., Soulaimani, A., Michard, A., 2008. The Pan-African belt. Continental Evolution: The Geology of Morocco. Springer Berlin Heidelberg, Berlin, Heidelberg, pp. 33–64 https://doi.org/10.1007/978-3-540-77076-3_2.

Godard, M., Bodinier, J.-L., Vasseur, G., 1995. Effects of mineralogical reactions on trace element redistributions in mantle rocks during percolation processes: a chromatographic approach. Earth Planet. Sci. Lett. 133, 449–461. https://doi.org/10.1016/0012-821X(95)00104-K.

Godard, M., Jousselin, D., Bodinier, J.-L., 2000. Relationships between geochemistry and structure beneath a palaeo-spreading centre: a study of the mantle section in the Oman ophiolite. Earth Planet. Sci. Lett. 180, 133–148.

Godard, M., Lagabrielle, Y., Alard, O., Harvey, J., 2008. Geochemistry of the highly depleted peridotites drilled at ODP Sites 1272 and 1274 (Fifteen-Twenty Fracture Zone, Mid-Atlantic Ridge): implications for mantle dynamics beneath a slow spreading ridge. Earth Planet. Sci. Lett. https://doi.org/10.1016/j.epsl.2007.11.058.

Gruau, G., Bernard-Griffiths, J., Lécuyer, C., 1998. The origin of U-shaped rare earth patterns in ophiolite peridotites: assessing the role of secondary alteration and melt/rock reaction. Geochim. Cosmochim. Acta 62, 3545–3560.

Hao, Y.-T., Xia, Q.-K., Tian, Z.-Z., Liu, J., Hao, Y.-T., Xia, Q.-K., Tian, Z.-Z., Liu, J., 2016. Mantle metasomatism did not modify the initial H2O content in peridotite xenoliths from the Tianchang basalts of eastern China. Lithos 260, 315–327. https://doi.org/10.1016/j.lithos.2016.06.003.

Hart, S.R., Zindler, A., 1986. In search of a bulk-Earth composition. Chem. Geol. 57, 247–267. https://doi.org/10.1016/0009-2541(86)90053-7.

Harvey, J., Savov, I.P., Agostini, S., Cliff, R.A., Walshaw, R., 2014. Si-metasomatism in serpentinized peridotite: the effects of talc-alteration on strontium and boron isotopes in abyssal serpentinites from Hole 1268a, ODP Leg 209. Geochim. Cosmochim. Acta 126, 30–48. https://doi.org/10.1016/j.gca.2013.10.035.

Hefferan, K., Soulaimani, A., Samson, S.D., Admou, H., Inglis, J., Saquaque, A., Heywood, N., 2014. A reconsideration of Pan African orogenic cycle in the Anti-Atlas Mountains, Morocco. J. Afr. Earth Sci. 98, 34–46. https://doi.org/10.1016/J.JAFREARSCI.2014.03.007.

Heuret, A., Lallemand, S., 2005. Plate motions, slab dynamics and back-arc deformation. Phys. Earth Planet. Inter. 149, 31–51. https://doi.org/10.1016/J.PEPI.2004.08.022.

Hickey-Vargas, R., Yogodzinski, G.M., Ishizuka, O., McCarthy, A., Bizimis, M., Kusano, Y., Savov, I.P., Arculus, R., 2018. Origin of depleted basalts during subduction initiation and early development of the Izu-Bonin-Mariana island arc: evidence from IODP expedition 351 site U1438, Amami-Sankaku basin. Geochim. Cosmochim. Acta 229, 85–111. https://doi.org/10.1016/J.GCA.2018.03.007.

Hochstaedter, A., Gill, J., Peters, R., Broughton, P., Holden, P., Taylor, B., 2001. Across-arc geochemical trends in the Izu-Bonin arc: contributions from the subducting slab. Geochem. Geophys. Geosyst. 2. https://doi.org/10.1029/2000GC000105 (n/a-n/a).

Hodel, F., Macouin, M., Triantafyllou, A., Carlut, J., Berger, J., Rousse, S., Ennih, N., Trindade, R.I.F., 2017. Unusual massive magnetite veins and highly altered Cr-spinels as relics of a Cl-rich acidic hydrothermal event in Neoproterozoic serpentinites (Bou Azzer ophiolite, Anti-Atlas, Morocco). Precambrian Res. 300, 151–167. https://doi.org/10.1016/j.precamres.2017.08.005.

Hodel, F., Macouin, M., Trindade, R.I.F., Triantafyllou, A., Ganne, J., Chavagnac, V., Berger, J., Rospabé, M., Destrigneville, C., Carlut, J., Ennih, N., Agrinier, P., 2018. Fossil black smoker yields oxygen isotopic composition of Neoproterozoic seawater. Nat. Commun. https://doi.org/10.1038/s41467-018-03890-w.

Hoskin, P.W.O., Schaltegger, U., 2003. The composition of zircon and igneous and metamorphic petrogenesis. Rev. Mineral. Geochem. 53, 27–62. https://doi.org/10.2113/0530027.

Inglis, J.D., MacLean, J.S., Samson, S.D., D'Lemos, R.S., Admou, H., Hefferan, K., 2004. A precise U–Pb zircon age for the Bleïda granodiorite, Anti-Atlas, Morocco: implications for the timing of deformation and terrane assembly in the eastern Anti-Atlas. J. Afr. Earth Sci. 39, 277–283. https://doi.org/10.1016/J.JAFREARSCI.2004.07.041.

Ishii, T., Robinson, P.T., Maekawa, H., Fiske, R., 1992. Petrological studies of peridotites from diapiric serpentinite seamounts in the Izu-Ogasawara-Mariana Forearc, Leg 125. Proceedings of the Ocean Drilling Program, 125 Scientific Results. Ocean Drilling Program, pp. 445–486 https://doi.org/10.2973/odp.proc.sr.125.129.1992.

Iyer, K., Austrheim, H., John, T., Jamtveit, B., 2008. Serpentinization of the oceanic lithosphere and some geochemical consequences: constraints from the Leka Ophiolite Complex, Norway. Chem. Geol. 249, 66–90. https://doi.org/10.1016/j.chemgeo.2007.12.005.

Jagoutz, E., Palme, H., Baddenhausen, H., Blum, K., Cendales, M., Dreibus, G., Spettel, B., Lorenz, V., Wänke, H., 1979. The abundance of major, minor and trace elements in the Earth's mantle as derived from primitive ultramafic nodules. Proc. Lunar Planet. Sci. Conf. 10th 2031–2050.

Janecky, D.R., Seyfried, W.E., 1986. Hydrothermal serpentinization of peridotite within the oceanic crust: experimental investigations of mineralogy and major element chemistry. Geochim. Cosmochim. Acta 50, 1357–1378. https://doi.org/10.1016/0016-7037(86)90311-X.

Kelemen, P.B., Koga, K., Shimizu, N., 1997. Geochemistry of gabbro sills in the crust-mantle transition zone of the Oman ophiolite: implications for the origin of the oceanic lower crust. Earth Planet. Sci. Lett. 146, 475–488. https://doi.org/10.1016/S0012-821X(96)00235-X.

Kodolányi, J., Pettke, T., Spandler, C., Kamber, B.S., Gméling, K., 2012. Geochemistry of ocean floor and fore-arc serpentinites: constraints on the ultramafic input to subduction zones. J. Petrol. 53, 235–270. https://doi.org/10.1093/petrology/egr058.

Kogiso, T., Tatsumi, Y., Nakano, S., 1997. Trace element transport during dehydration processes in the subducted oceanic crust: 1. Experiments and implications for the origin of ocean island basalts. Earth Planet. Sci. Lett. 148 (1–2), 193–205.

Kydonakis, K., Kostopoulos, D., Poujol, M., Brun, J.P., Papanikolaou, D., Paquette, J.L., 2014. The dispersal of the Gondwana Super-fan System in the eastern Mediterranean: new insights from detrital zircon geochronology. Gondwana Res. 25, 1230–1241. https://doi.org/10.1016/j.gr.2013.05.009.

Leake, B.E., Woolley, A.R., Birch, W.D., Burke, E.A.J., Ferraris, G., Grice, J.D., Hawthorne, F.C., Kisch, H.J., Krivovichev, V.G., Schumacher, J.C., Stephenson, N.C.N., Whittaker, E.J.W., 2004. Nomenclature of amphiboles: additions and revisions to the International Mineralogical Association's amphibole nomenclature. Am. Mineral. 89, 883–887. https://doi.org/10.1180/0026461046810182.

Leblanc, M., 1975. Ophiolites précambriennes et gites arséniés de Cobalt (Bou Azzer - Maroc). Université Paris VI, Paris.

Leblanc, M., 1981. Chapter 17 the Late Proterozoic ophiolites of Bou Azzer (Morocco): evidence for Pan-African plate tectonics. Dev. Precambrian Geol. 4, 435–451. https://doi.org/10.1016/S0166-2635(08)70022-7.

Li, Z.X., Bogdanov, S.V., Collins, A.S., Davidson, A., De Waele, B., Ernst, R.E., Fitzsimons, I.C.W., Fuck, R.A., Gladkochub, D.P., Jacobs, J., Karlstrom, K.E., Lu, S., Natapov, L.M., Pease, V., Pisarevsky, S.A., Thrane, K., Vernikovsky, V., 2008. Assembly, configuration, and break-up history of Rodinia: a synthesis. Precambrian Res. 160, 179–210.

MacLeod, C.J., Johan Lissenberg, C., Bibby, L.E., 2013. "Moist MORB" axial magmatism in the Oman ophiolite: the evidence against a mid-ocean ridge origin. Geology 41, 459–462. https://doi.org/10.1130/G33904.1.

Malvoisin, B., 2015. Mass transfer in the oceanic lithosphere: serpentinization is not isochemical. Earth Planet. Sci. Lett. 430, 75–85. https://doi.org/10.1016/j.epsl.2015.07.043.

Marchesi, C., Garrido, C.J., Godard, M., Proenza, J.A., Gervilla, F., Blanco-Moreno, J., 2006. Petrogenesis of highly depleted peridotites and gabbroic rocks from the Mayarí-Baracoa Ophiolitic Belt (eastern Cuba). Contrib. Mineral. Petrol. 151, 717–736. https://doi.org/10.1007/s00410-006-0089-0.

Marchesi, C., Garrido, C.J., Godard, M., Belley, F., Ferré, E., 2009. Migration and accumulation of ultra-depleted subduction-related melts in the Massif du Sud ophiolite (New Caledonia). Chem. Geol. 266, 171–186. https://doi.org/10.1016/j.chemgeo.2009.06.004.

McDonough, W.F., Sun, S.-s., 1995. The composition of the Earth. Chem. Geol. 120, 223–253. https://doi.org/10.1016/0009-2541(94)00140-4.

Miyashiro, A., Shido, F., Ewing, M., 1969. Composition and origin of serpentinites from the Mid-Atlantic Ridge near 24° and 30° North Latitude. Contrib. Mineral. Petrol. 23, 117–127. https://doi.org/10.1007/BF00375173.

Müller, R.D., Sdrolias, M., Gaina, C., Roest, W.R., 2008. Age, spreading rates, and spreading asymmetry of the world's ocean crust. Geochem. Geophys. Geosyst. 9. https://doi.org/10.1029/2007GC001743 (n/a-n/a).

Naidoo, D.D., Bloomer, S.H., Saquaque, A., Hefferan, K., 1991. Geochemistry and significance of metavolcanic rocks from the Bou Azzer-El Graara ophiolite (Morocco). Precambrian Res. 53, 79–97.

Navon, O., Stolper, E., 1987. Geochemical consequences of melt percolation: the upper mantle as a chromatographic column. J. Geol. 95, 285–307. https://doi.org/10.1086/629131.

Niu, Y., 2004. Bulk-rock major and trace element compositions of abyssal peridotites: implications for mantle melting, melt extraction and post-melting processes beneath mid-ocean ridges. J. Petrol. 45. https://doi.org/10.1093/petrology/egh068.

Palandri, J.L., Reed, M.H., 2004. Geochemical models of metasomatism in ultramafic systems: serpentinization, rodingitization, and sea floor carbonate chimney precipitation. Geochim. Cosmochim. Acta 68, 1115–1133. https://doi.org/10.1016/j.gca.2003.08.006.

Pallister, J.S., Knight, R.J., 1981. Rare-earth element geochemistry of the Samail Ophiolite near Ibra, Oman. J. Geophys. Res. Solid Earth 86, 2673–2697. https://doi.org/10.1029/JB086iB04p02673.

Parkinson, I.J., Pearce, J.A., 1998. Peridotites from the Izu-Bonin-Mariana Forearc (ODP Leg 125): evidence for mantle melting and melt-mantle interaction in a supra-subduction zone setting. J. Petrol. 39, 1577–1618. https://doi.org/10.1093/petroj/39.9.1577.

Paulick, H., Bach, W., Godard, M., De Hoog, J.C.M., Suhr, G., Harvey, J., 2006. Geochemistry of abyssal peridotites (Mid-Atlantic Ridge, 15°20′N, ODP Leg 209): implications for fluid/rock interaction in slow spreading environments. Chem. Geol. 234, 179–210. https://doi.org/10.1016/j.chemgeo.2006.04.011.

Pearce, J.A., 2008. Geochemical fingerprinting of oceanic basalts with applications to ophiolite classification and the search for Archean oceanic crust. Lithos 100, 14–48. https://doi.org/10.1016/J.LITHOS.2007.06.016.

Pearce, J.A., Stern, R.J., 2006. Origin of Back-arc Basin Magmas: Trace Element and Isotope Perspectives. American Geophysical Union, pp. 63–86 https://doi.org/10.1029/166GM06.

Pearce, J.A., Barker, P.F., Edwards, S.J., Parkinson, I.J., Leat, P.T., 2000. Geochemistry and tectonic significance of peridotites from the South Sandwich arc-basin system, South Atlantic. Contrib. Mineral. Petrol. 139, 36–53. https://doi.org/10.1007/s004100050572.

Pearce, J.A., Stern, R.J., Bloomer, S.H., Fryer, P., 2005. Geochemical mapping of the Mariana arc-basin system: implications for the nature and distribution of subduction components. Geochem. Geophys. Geosyst. 6. https://doi.org/10.1029/2004GC000895 (n/a-n/a).

Prinzhofer, A., Allègre, C.J., 1985. Residual peridotites and the mechanisms of partial melting. Earth Planet. Sci. Lett. 74, 251–265. https://doi.org/10.1016/0012-821X(85)90025-1.

Reagan, M.K., Ishizuka, O., Stern, R.J., Kelley, K.A., Ohara, Y., Blichert-Toft, J., Bloomer, S.H., Cash, J., Fryer, P., Hanan, B.B., Hickey-Vargas, R., Ishii, T., Kimura, J.-I., Peate, D.W., Rowe, M.C., Woods, M., 2010. Fore-arc basalts and subduction initiation in the Izu-Bonin-Mariana system. Geochem. Geophys. Geosyst. 11. https://doi.org/10.1029/2009GC002871 (n/a-n/a).

Reagan, M.K., Pearce, J.A., Petronotis, K., Almeev, R.R., Avery, A.J., Carvallo, C., Chapman, T., Christeson, G.L., Ferré, E.C., Godard, M., Heaton, D.E., Kirchenbaur, M., Kurz, W., Kutterolf, S., Li, H., Li, Y., Michibayashi, K., Morgan, S., Nelson, W.R., Prytulak, J., Python, M., Robertson, A.H.F., Ryan, J.G., Sager, W.W., Sakuyama, T., Shervais, J.W., Shimizu, K., Whattam, S.A., 2017. Subduction initiation and ophiolite crust: new insights from IODP drilling. Int. Geol. Rev. 59, 1439–1450. https://doi.org/10.1080/00206814.2016.1276482.

Saka, S., Uysal, I., Akmaz, R.M., Kaliwoda, M., Hochleitner, R., Saka, S., Uysal, I., Akmaz, R.M., Kaliwoda, M., Hochleitner, R., 2014. The effects of partial melting, melt–mantle interaction and fractionation on ophiolite generation: constraints from the late Cretaceous Pozantı-Karsantı ophiolite, southern Turkey. Lithos 202–203, 300–316. https://doi.org/10.1016/j.lithos.2014.05.027.

Samson, S.D., Inglis, J.D., D'Lemos, R.S., Admou, H., Blichert-Toft, J., Hefferan, K., 2004. Geochronological, geochemical, and Nd–Hf isotopic constraints on the origin of Neoproterozoic plagiogranites in the Tasriwine ophiolite, Anti-Atlas orogen, Morocco. Precambrian Res. 135, 133–147. https://doi.org/10.1016/j.precamres.2004.08.003.

Saquaque, A., Admou, H., Karson, J., Hefferan, K., Reuber, I., 1989. Precambrian accretionary tectonics in the Bou Azzer-El Graara region, Anti-Atlas, Morocco. Geology 17, 1107. https://doi.org/10.1130/0091-7613(1989)017<1107:PATITB>2.3.CO;2.

Savov, I.P., Ryan, J.G., D'Antonio, M., Kelley, K., Mattie, P., 2005. Geochemistry of serpentinized peridotites from the Mariana Forearc Conical Seamount, ODP Leg 125: implications for the elemental recycling at subduction zones. Geochem. Geophys. Geosyst. 6. https://doi.org/10.1029/2004GC000777 (n/a-n/a).

Savov, I.P., Ryan, J.G., D'Antonio, M., Fryer, P., 2007. Shallow slab fluid release across and along the Mariana arc-basin system: insights from geochemistry of serpentinized peridotites from the Mariana fore arc. J. Geophys. Res. 112, B09205. https://doi.org/10.1029/2006JB004749.

Schoene, B., Bowring, S.A., 2007. Determining accurate temperature–time paths from U–Pb thermochronology: an example from the Kaapvaal craton, southern Africa. Geochim. Cosmochim. Acta 71, 165–185. https://doi.org/10.1016/J.GCA.2006.08.029.

Shinjo, R., Chung, S.-L., Kato, Y., Kimura, M., 1999. Geochemical and Sr-Nd isotopic characteristics of volcanic rocks from the Okinawa Trough and Ryukyu Arc: implications for the evolution of a young, intracontinental back arc basin. J. Geophys. Res. Solid Earth 104, 10591–10608. https://doi.org/10.1029/1999JB900040.

Snow, J.E., Dick, H.J.B., 1995. Pervasive magnesium loss by marine weathering of peridotite. Geochim. Cosmochim. Acta 59, 4219–4235. https://doi.org/10.1016/0016-7037(95)00239-V.

Soulaimani, A., Jaffal, M., Maacha, L., Kchikach, A., Najine, A., Saidi, A., 2006. Modélisation magnétique de la suture ophiolitique de Bou Azzer–El Graara (Anti-Atlas central, Maroc). Implications sur la reconstitution géodynamique panafricaine. Compt. Rendus Geosci. 338, 153–160.

Soulaimani, A., Ouanaimi, H., Baidder, L., 2018. The Anti-Atlas Pan-African Belt (Morocco): overview and pending questions. Compt. Rendus Geosci. 350, 279–288. https://doi.org/10.1016/J.CRTE.2018.07.002.

Stern, R.J., 2005. Evidence from ophiolites, blueschists, and ultrahigh-pressure metamorphic terranes that the modern episode of subduction tectonics began in Neoproterozoic time. Geology 33, 557. https://doi.org/10.1130/G21365.1.

Stern, R.J., Reagan, M., Ishizuka, O., Ohara, Y., Whattam, S., 2012. To understand subduction initiation, study forearc crust: to understand forearc crust, study ophiolites. Lithosphere 4, 469–483. https://doi.org/10.1130/L183.1.

Sun, S.-s., McDonough, W.F., 1989. Chemical and isotopic systematics of oceanic basalts: implications for mantle composition and processes. Geol. Soc. Lond. Spec. Publ. 42.

Taylor, B., Martinez, F., 2003. Back-arc basin basalt systematics. Earth Planet. Sci. Lett. 210, 481–497. https://doi.org/10.1016/S0012-821X(03)00167-5.

Thomas, R.J., Chevallier, L.P., Gresse, P.G., Harmer, R.E., Eglington, B.M., Armstrong, R.A., de Beer, C.H., Martini, J.E.J., de Kock, G.S., Macey, P.H., Ingram, B.A., 2002. Precambrian evolution of the Sirwa Window, Anti-Atlas Orogen, Morocco. Precambrian Res. 118, 1–57. https://doi.org/10.1016/S0301-9268(02)00075-X.

Tian, L., Castillo, P.R., Hawkins, J.W., Hilton, D.R., Hanan, B.B., Pietruszka, A.J., 2008. Major and trace element and Sr–Nd isotope signatures of lavas from the Central Lau Basin: implications for the nature and influence of subduction components in the back-arc mantle. J. Volcanol. Geotherm. Res. 178, 657–670. https://doi.org/10.1016/j.jvolgeores.2008.06.039.

Tollstrup, D., Gill, J., Kent, A., Prinkey, D., Williams, R., Tamura, Y., Ishizuka, O., 2010. Across-arc geochemical trends in the Izu-Bonin arc: contributions from the subducting slab, revisited. Geochem. Geophys. Geosyst. 11. https://doi.org/10.1029/2009GC002847@10.1002/(ISSN)1525-2027.IZUBONIN1.

Triantafyllou, A., Berger, J., Diot, H., Ennih, N., Plissart, G., 2012. Panafrican obduction, crushing & shearing of the Neoproterozoic Khzama ophiolite (Anti-Atlas, Morocco). 4th International Geologica Belgica Meeting, 11–14 Sept, Brussels, Belgium.

Triantafyllou, A., Berger, J., Baele, J.-M., Diot, H., Ennih, N., Plissart, G., Monnier, C., Watlet, A., Bruguier, O., Spagna, P., Vandycke, S., 2016. The Tachakoucht–Iriri–Tourtit arc complex (Moroccan Anti-Atlas): Neoproterozoic records of polyphased subduction-accretion dynamics during the Pan-African orogeny. J. Geodyn. 96, 81–103. https://doi.org/10.1016/j.jog.2015.07.004.

Triantafyllou, A., Watlet, A., Bastin, C., 2017. Geolokit: an interactive tool for visualising and exploring geoscientific data in Google Earth. Int. J. Appl. Earth Obs. Geoinf. 62, 39–46. https://doi.org/10.1016/j.jag.2017.05.011.
Triantafyllou, A., Berger, J., Baele, J.-M., Bruguier, O., Diot, H., Ennih, N., Monnier, C., Plissart, G., Vandycke, S., Watlet, A., 2018. Intra-oceanic arc growth driven by magmatic and tectonic processes recorded in the Neoproterozoic Bougmane arc complex (Anti-Atlas, Morocco). Precambrian Res. 304, 39–63. https://doi.org/10.1016/j.precamres.2017.10.022.
Triantafyllou, A., Berger, J., Baele, J.M., Mattielli, N., Ducea, M.N., Sterckx, S., Ennih, N., 2020. Episodic magmatism during the growth of a Neoproterozoic oceanic arc (Anti-Atlas, Morocco). Precambrian Res. 339, 105610.
Ulrich, M., Picard, C., Guillot, S., Chauvel, C., Cluzel, D., Meffre, S., 2010. Multiple melting stages and refertilization as indicators for ridge to subduction formation: the New Caledonia ophiolite. Lithos 115, 223–236. https://doi.org/10.1016/j.lithos.2009.12.011.
Uysal, İ., Ersoy, E.Y., Karslı, O., Dilek, Y., Sadıklar, M.B., Ottley, C.J., Tiepolo, M., Meisel, T., 2012. Coexistence of abyssal and ultra-depleted SSZ type mantle peridotites in a Neo-Tethyan Ophiolite in SW Turkey: constraints from mineral composition, whole-rock geochemistry (major–trace–REE–PGE), and Re–Os isotope systematics. Lithos 132, 50–69. https://doi.org/10.1016/j.lithos.2011.11.009.
Uysal, I., Ersoy, E.Y., Dilek, Y., Escayola, M., Sarıfakıoğlu, E., Saka, S., Hirata, T., 2015. Depletion and refertilization of the Tethyan oceanic upper mantle as revealed by the early Jurassic Refahiye ophiolite, NE Anatolia—Turkey. Gondwana Res. 27, 594–611. https://doi.org/10.1016/j.gr.2013.09.008.
Uysal, I., Ersoy, E.Y., Dilek, Y., Kapsiotis, A., Sarıfakıoğlu, E., 2016. Multiple episodes of partial melting, depletion, metasomatism and enrichment processes recorded in the heterogeneous upper mantle sequence of the Neotethyan Eldivan ophiolite, Turkey. Lithos 246, 228–245. https://doi.org/10.1016/j.lithos.2016.01.004.
Vermeesch, P., 2018. Isoplot R: a free and open toolbox for geochronology. Geosci. Front. 9, 1479–1493. https://doi.org/10.1016/J.GSF.2018.04.001.
Vernières, J., Godard, M., Bodinier, J.-L., 1997. A plate model for the simulation of trace element fractionation during partial melting and magma transport in the Earth's upper mantle. J. Geophys. Res. Solid Earth 102, 24771–24784. https://doi.org/10.1029/97JB01946.
Walsh, G.J., Benziane, F., Aleinikoff, J.N., Harrison, R.W., Yazidi, A., Burton, W.C., Quick, J.E., Saadane, A., 2012. Neoproterozoic tectonic evolution of the Jebel Saghro and Bou Azzer—El Graara inliers, eastern and central Anti-Atlas, Morocco. Precambrian Res. 216, 23–62. https://doi.org/10.1016/j.precamres.2012.06.010.
Warren, J.M., 2016. Global variations in abyssal peridotite compositions. Lithos 248–251, 193–219. https://doi.org/10.1016/j.lithos.2015.12.023.
Warren, J.M., Shimizu, N., 2010. Cryptic variations in abyssal peridotite compositions: evidence for shallow-level melt infiltration in the oceanic lithosphere. J. Petrol. 51, 395–423. https://doi.org/10.1093/petrology/egp096.
Winchester, J.A., Floyd, P.A., 1977. Geochemical discrimination of different magma series and their differentiation products using immobile elements. Chem. Geol. 20, 325–343. https://doi.org/10.1016/0009-2541(77)90057-2.
Woelki, D., Regelous, M., Haase, K.M., Romer, R.H.W., Beier, C., 2018. Petrogenesis of boninitic lavas from the Troodos Ophiolite, and comparison with Izu–Bonin–Mariana fore-arc crust. Earth Planet. Sci. Lett. 498, 203–214. https://doi.org/10.1016/j.epsl.2018.06.041.
Workman, R.K., Hart, S.R., 2005. Major and trace element composition of the depleted MORB mantle (DMM). Earth Planet. Sci. Lett. 231, 53–72. https://doi.org/10.1016/j.epsl.2004.12.005.
You, C., Castillo, P., Gieskes, J., Chan, L., 1996. Trace element behavior in hydrothermal experiments: implications for fluid processes at shallow depths in subduction zones. Earth Planet.
Zou, H., 2007. Quantitative Geochemistry. Imperial College Press.